cmgh
CELLULAR AND MOLECULAR GASTROENTEROLOGY AND HEPATOLOGY

ORIGINAL RESEARCH

The Circadian Clock Gene, *Bmal1*, Regulates Intestinal Stem Cell Signaling and Represses Tumor Initiation

Kyle Stokes,[1] Malika Nunes,[1] Chantelle Trombley,[1] Danilo E. F. L. Flôres,[2] Gang Wu,[2] Zainab Taleb,[1] Abedalrhman Alkhateeb,[3] Suhrid Banskota,[4] Chris Harris,[5] Oliver P. Love,[5] Waliul I. Khan,[4] Luis Rueda,[3] John B. Hogenesch,[2] and Phillip Karpowicz[1]

[1]*Department of Biomedical Sciences, University of Windsor, Windsor, Ontario, Canada;* [2]*Division of Human Genetics and Immunobiology, Cincinnati Children's Hospital Medical Center,Cincinnati, Ohio;* [3]*School of Computer Science, University of Windsor, Windsor, Ontario, Canada;* [4]*Department of Pathology and Molecular Medicine, Farncombe Family Digestive Health Research Institute, McMaster University, Hamilton, Ontario, Canada;* [5]*Department of Integrative Biology, University of Windsor, Windsor, Ontario, Canada*

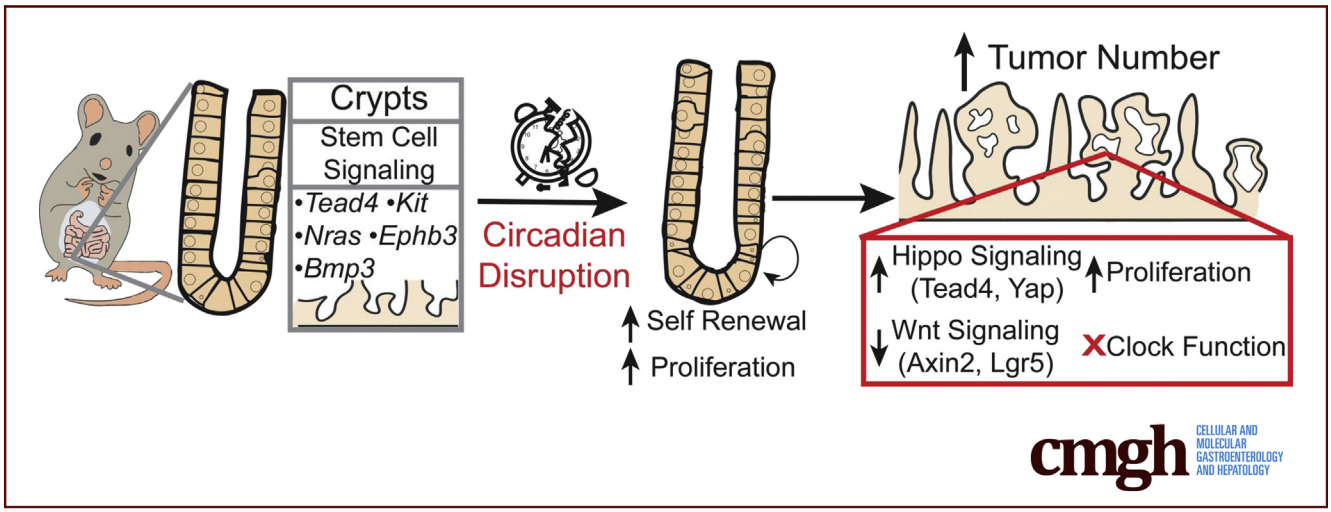

SUMMARY

The loss of circadian rhythms in the intestine leads to aberrant regulation of stem cell signaling pathways and increased tumor initiation.

BACKGROUND & AIMS: Circadian rhythms are daily physiological oscillations driven by the circadian clock: a 24-hour transcriptional timekeeper that regulates hormones, inflammation, and metabolism. Circadian rhythms are known to be important for health, but whether their loss contributes to colorectal cancer is not known. We tested the nonredundant clock gene *Bmal1* in intestinal homeostasis and tumorigenesis, using the Apc^{min} model of colorectal cancer.

METHODS: *Bmal1* mutant, epithelium-conditional *Bmal1* mutant, and photoperiod (day/night cycle) disrupted mice bearing the Apc^{min} allele were assessed for tumorigenesis. Tumors and normal nontransformed tissue were characterized. Intestinal organoids were assessed for circadian transcription rhythms by RNA sequencing, and in vivo and organoid assays were used to test *Bmal1*-dependent proliferation and self-renewal.

RESULTS: Loss of *Bmal1* or circadian photoperiod increases tumor initiation. In the intestinal epithelium the clock regulates transcripts involved in regeneration and intestinal stem cell signaling. Tumors have no self-autonomous clock function and only weak clock function in vivo. Apc^{min} clock-disrupted tumors show high Yes-associated protein 1 (Hippo signaling) activity but show low Wnt (Wingless and Int-1) activity. Intestinal organoid assays show that loss of *Bmal1* increases self-renewal in a Yes-associated protein 1–dependent manner.

CONCLUSIONS: *Bmal1* regulates intestinal stem cell pathways, including Hippo signaling, and the loss of circadian rhythms potentiates tumor initiation. Transcript profiling: GEO accession number: GSE157357. *(Cell Mol Gastroenterol Hepatol 2021;■:■–■; https://doi.org/10.1016/j.jcmgh.2021.08.001)*

Keywords: Circadian Rhythms; Intestinal Stem Cells; Colorectal Cancer; Hippo Pathway.

Cancer is a disease that commences with the initiation of tumors, and progresses when hyperproliferative tumor cells develop into increasingly malignant phenotypes.[1] How the body's physiology precisely

contributes to tumor initiation vs progression is not clear. Circadian rhythms are daily changes in physiology driven by the circadian clock: a self-sustaining, 24-hour, transcriptional feedback mechanism comprising the transcription factors *Clock/Bmal1* and their repressors *Per1-3/Cry1-2*.[2] In addition to this core mechanism, a regulatory loop composed of *Nr1d1-2* regulates the transcription of *Bmal1* to confer robustness; post-transcriptional, translational, and epigenetic mechanisms also affect circadian clock function.[2] Self-sustaining daily changes in the abundance and activity of the core clock components underlies 24-hour transcriptional rhythms that are present in nearly all cells of the body, where more than 40% of the genome is rhythmic.[3] In doing so, the clock is thought to coordinate the timing of compatible and incompatible physiological processes throughout the body, thereby maximizing health and fitness. Daily circadian rhythms in hormones, inflammation, and metabolic processes are essential to health,[4,5] and are the same physiological processes often dysregulated in tumor cells.[1]

Circadian disruption, an outcome of frequent activities such as shift work, increases cancer incidence,[6–10] and therefore a link between circadian rhythms and cancer has been actively sought.[11–14] Cancers can harbor abnormal expression or mutations in circadian genes,[15–17] but the circadian rhythmicity of cancers has not been established. For instance, breast cancer cells have been shown to have normal[18] or abnormal circadian gene expression,[19] raising the question of whether certain cancerous clones are clock-dead, or whether clock function is correlated with different stages of malignancy. Loss of circadian clock activity leads to cellular changes such as disruptions in metabolism,[20,21] cell cycle,[22,23] apoptosis,[24,25] and the DNA damage response,[26,27] cellular processes whose dysfunction are known to be protumorigenic. Animal models have shown that the loss of clock genes increases cancer,[28–31] although it is worth noting that questions have been raised about the strains of mice used in these studies,[11,14,32] as well as discrepancies in tumorigenesis noted between different clock mutants.[13,14] In addition to the circadian clock as a transcriptional regulator, environmental factors that cause circadian disruption are complex and involve dysfunction in the orchestration of body-wide processes.[33] Thus, the effect of circadian rhythms on colorectal cancer are poorly understood. How does the complete loss of circadian rhythms in the body, vs loss at the cellular level, lead to tumor initiation or progression? This is an important question, relevant in the role of circadian health as a factor in colorectal cancer prevention and treatment.

To test the role of the clock in colorectal tumorigenesis, we used the Apc^{min} mouse strain, which models human colorectal cancer in a mechanistically conserved manner.[34,35] This strain has only 1 functional copy of the gene *Apc*: intestinal epithelial cells in these mice can undergo spontaneous loss of heterozygosity of the remaining allele and subsequent tumor initiation events at random positions in the epithelium. *Apc* mutant tumor-initiating cells are reminiscent of proliferative intestinal stem cells (ISCs),[36,37] which divide throughout life to produce differentiated intestinal cells and regenerate intestinal epithelia.[38] This is because the *Apc* gene is a negative regulator of Wnt signaling, a pathway required for the maintenance and proliferation of Lgr5+ (Leucine-rich repeat-containing G-protein coupled receptor 5) ISCs. Inflammation is also a critical factor in regeneration,[39] and potent driver of tumorigenesis in the intestine.[40] Recent studies have shown that intestinal cells can assume a fetal-like state during regeneration,[41,42] and inflammation can activate the Hippo tumor-suppressor pathway to promote regeneration.[42–45] Thus, both the Wnt and Hippo pathways are regenerative factors that are co-opted during tumorigenesis to drive tumor growth.

We previously showed that regeneration, in both *Drosophila* and mice, is regulated by the circadian clock.[46–48] ISCs show 24-hour proliferation and cell signaling characteristic of circadian rhythmicity, and loss of clock function causes arrhythmic and dysfunctional regeneration. These same processes are regulated by the clock in epidermal stem cells, suggesting they are conserved in epithelia.[49] We hypothesized that complete loss of circadian rhythms would increase intestinal tumorigenesis. Congenic Apc^{min} mice lacking *Bmal1* have a 2-fold higher tumor initiation probability, which is recapitulated in Apc^{min} mice housed under constant light. In the intestinal epithelium, the circadian clock regulates a small number of rhythmic genes, including the Hippo signaling pathway transducer *Tead4*. However, Apc^{min} tumors show reduced circadian rhythms in vivo, and tumor cells have no capacity to generate cell-autonomous circadian rhythms in vitro, showing that loss of rhythms is linked to. tumorigenesis. Furthermore, clock-dead Apc^{min} + *Bmal1* mutant tumor organoids down-regulate the Wnt pathway and up-regulate the Hippo pathway, and show increased Hippo-dependent self-renewal. Our results show that the circadian clock is a physiological repressor of early tumor-initiation events, and that the core clock gene *Bmal1* participates in the remodeling of stem cell–regenerative signaling pathways in the epithelium.

Results

Loss of Bmal1 *Increases Tumor Initiation in the Intestine*

$Bmal1^{-/-}$ mutant mice are viable littermates from heterozygous crosses but show no circadian rhythms or clock activity.[50] We crossed Apc^{min} mice on a *C57BL/6* background with $Bmal1^{-/-}$ null mutant mice also on a *C57BL/6* background, then offspring were backcrossed 7 generations

Abbreviations used in this paper: **ANOVA, analysis of variance; BH, Benjamini-Hochberg; cKO, conditional knockout; GSEA, Gene Set Enrichment Analysis; ISC, intestinal stem cell; Lgr5+, Leucine-rich repeat-containing G-protein coupled receptor 5; LL, constant light cycle; PBS, phosphate-buffered saline; PHH3, phosphorylated histone H-3; Tnf, tumor necrosis factor; Wnt, Wingless and Int-1; Yap, Yes-associated protein 1.**

2352-345X
https://doi.org/10.1016/j.jcmgh.2021.08.001

to create a congenic strain. Littermates from congenic heterozygous *Apc*$^{min/+}$; *Bmal1*$^{+/-}$ crosses were examined at 3 months of age to avoid age-related phenotypes.[51] *Bmal1*-deficient mice have low and arrhythmic serum levels of corticosterone, a known regulator of circadian physiology[52] consistent with previous findings (Figure 1*A*).[53] Large tumors (>1 mm) and small tumors (<1 mm) were quantified throughout the intestine. Control (*Apc*$^{+/+}$; *Bmal1*$^{+/+}$) mice had no tumors, and neither did the *Bmal1*$^{-/-}$ mice (*Apc*$^{+/+}$; *Bmal1*$^{-/-}$), indicating that the loss of *Bmal1* alone does not drive tumor initiation (Figure 1*B–D*). However, *Apc*^{min} + *Bmal1*$^{-/-}$ mice (*Apc*$^{min/+}$; *Bmal1*$^{-/-}$) develop 2 times more tumors compared with *Apc*^{min} controls (*Apc*$^{min/+}$; *Bmal1*$^{+/+}$) (Figure 1*B–D*). The presence of many small tumors suggests that tumorigenesis is higher in the absence of *Bmal1*.

We measured proliferation in intestinal crypts and tumors using Ki67, a marker of cell-cycle activity, and phosphorylated-histone H3 (PHH3), a marker of mitosis. *Apc*^{min} + *Bmal1*$^{-/-}$ intestinal crypts and tumors show stronger expression levels of Ki67 and an increased number of Ki67+ cells (Figures 1*E* and *F* and 2*A* and *B*). PHH3 cell number is increased in *Apc*^{min} + *Bmal1*$^{-/-}$ crypts and tumors and shows daily variation (Figures 1*G* and *H* and 2*E* and *F*). This indicates that loss of *Bmal1* increases proliferation in the *Apc*^{min} background. *Apc*^{min} + *Bmal1*$^{-/-}$ tissues also showed reduced cell death (Figures 1*I* and 2*G*), as marked by cleaved caspase-3. Histopathologic analysis showed that *Bmal1* loss slightly reduces dysplasia (Figure 1*J*), but does not affect tumor size (Figure 1*K*). To test whether tumor growth is increased in an age-dependent fashion, we examined mice at earlier stages of tumor initiation. One-month-old mice lacking *Bmal1* did not show an increase in tumor number yet (Figure 1*L* and *M*), but Ki67 expression levels and/or numbers were increased in tumors (Figure 1*N* and *O*) and in crypts (Figure 2*C* and *D*). Thus, the phenotype of *Bmal1* loss of function is the generation of more tumors through increased proliferation. We conclude that in this manner *Bmal1* negatively regulates tumorigenesis.

A recent study proposed that the circadian clock regulates the Wnt pathway ligand, Wnt3A, in the Paneth cells of intestinal organoids.[54] Because dysfunction of Wnt is a driver of tumorigenesis, we tested if increased Wnt signaling disruption precedes the increase in *Apc*^{min} + *Bmal1*$^{-/-}$ tumor initiation. β-catenin, the transducer of Wnt signaling, was unaltered (Figure 2*H* and *I*). *Apc*^{min} + *Bmal1*$^{-/-}$ untransformed crypts showed reductions in the number (Figure 2*J*) and size (Figure 2*K*) of crypts, but an increase in the overall number of crypt cells present (Figure 2*L*). These changes did not resemble the heightened proliferation that would be expected from Wnt increased activity. However, we found an increase in the production of secretory cell types, including Paneth cells (lysozyme-positive) and goblet cells (Alcian Blue) in the *Apc*^{min} + *Bmal1*$^{-/-}$ intestine (Figure 2*M–P*). These data are consistent with previous reports showing Hippo pathway effects on secretory cell differentiation.[43,55]

The Normal Epithelium Shows Self-Sustaining Circadian Clock Function, but Tumors Do Not

To test how *Bmal1* functions as a transcriptional regulator in the epithelial crypt, we derived organoids from congenic wild-type control mice (*Apc*$^{+/+}$; *Bmal1*$^{+/+}$) vs *Bmal1*$^{-/-}$ mice (*Apc*$^{+/+}$; *Bmal1*$^{-/-}$). Twelve hours after passaging, organoids were synchronized using a single pulse of the glucocorticoid dexamethasone,[46] and then fractions were collected every 2 hours from 24 to 48 hours after synchronization to avoid immediate early response gene effects.[56] RNA was sequenced, and transcriptomes were analyzed by MetaCycle[57] (Figure 3*A*). Comparing wild-type vs *Bmal1*$^{-/-}$ organoid circadian expression showed that only 41 genes are expressed rhythmically in a *Bmal1*-dependent manner (base expression, >0.5; relative amplitude, >0.05; BH (Benjamini-Hochberg), q <0.1) (Figure 3*B*, Supplementary Table 1). These include well-known circadian clock components such as *Bmal1* itself, *Nr1d1-2*, *Nr1f3*, *Per3*, *Cry1-2*, and *Tef* (Figure 3*C*, Supplementary Table 1). Additional rhythmic targets, previously implicated in ISC biology, are notable including the markers: *Anxa2*, *7*, *8*[58]; differentiation regulators: *Bmp3*, *Cav2*, *EphB3*[36]; growth regulators: *Nras*[1]; DNA repair component: *Parp3*[58]; and regeneration regulators: *Kit* and *Tead4*[55,59] (Figure 3*C*, Supplementary Table 1). No cell-cycle regulators were detected. A second organoid assay, performed over 2 days to test a subset of the top rhythmic genes, showed that circadian clock genes showed consistent self-sustaining 24-hour rhythms (Figure 3*D*). However, the Hippo pathway component *Tead4* showed time-dependent variation that had less consistent 24-hour rhythmicity. These results suggest that *Bmal1* regulates clock transcription in the normal intestinal epithelium, but that its targets are limited to a small number of genes that include several known ISC regulators.

We performed the same experiment using *Apc*^{min} control organoids (*Apc*$^{min/+}$; *Bmal1*$^{+/+}$) and *Apc*^{min} + *Bmal1*$^{-/-}$ organoids (*Apc*$^{min/+}$; *Bmal1*$^{-/-}$) derived from microdissected tumors (Figure 4*A*). *Apc*^{min} organoids express 238 rhythmic genes and *Apc*^{min} + *Bmal1*$^{-/-}$ express 263, using the same criteria as described earlier (Figure 4*B*, Supplementary Table 1). The circadian clock was dysfunctional in both genotypes. Even control tumors with wild-type *Bmal1* do not have self-sustaining circadian clock transcription, indeed these down-regulate most clock components (Supplementary Table 2). Only 4 rhythmic genes overlapped between genotypes, showing that the 24-hour variation in gene expression is unique (Figure 4*C*). The top genes in *Apc*^{min} (*Golga1*, *Dolk*, *Rnf128*) or *Apc*^{min} + *Bmal1*$^{-/-}$ (*Mlxipl*, *Msmo1*, *Fam76b*) were tested over 2 days, and although some showed variation over 24-hour organoid culture (Figure 4*D*), these were not self-sustaining circadian rhythms over 48 hours, suggesting stochastic expression, with the exception of *Rnf128* and *Msmo1*, which have 24-hour rhythms (Figure 4*E*). We conclude that tumor organoids show 24-hour variation in gene expression, independent of *Bmal1*, but have no autonomous, self-sustaining, rhythmic, transcriptional clock mechanism present.

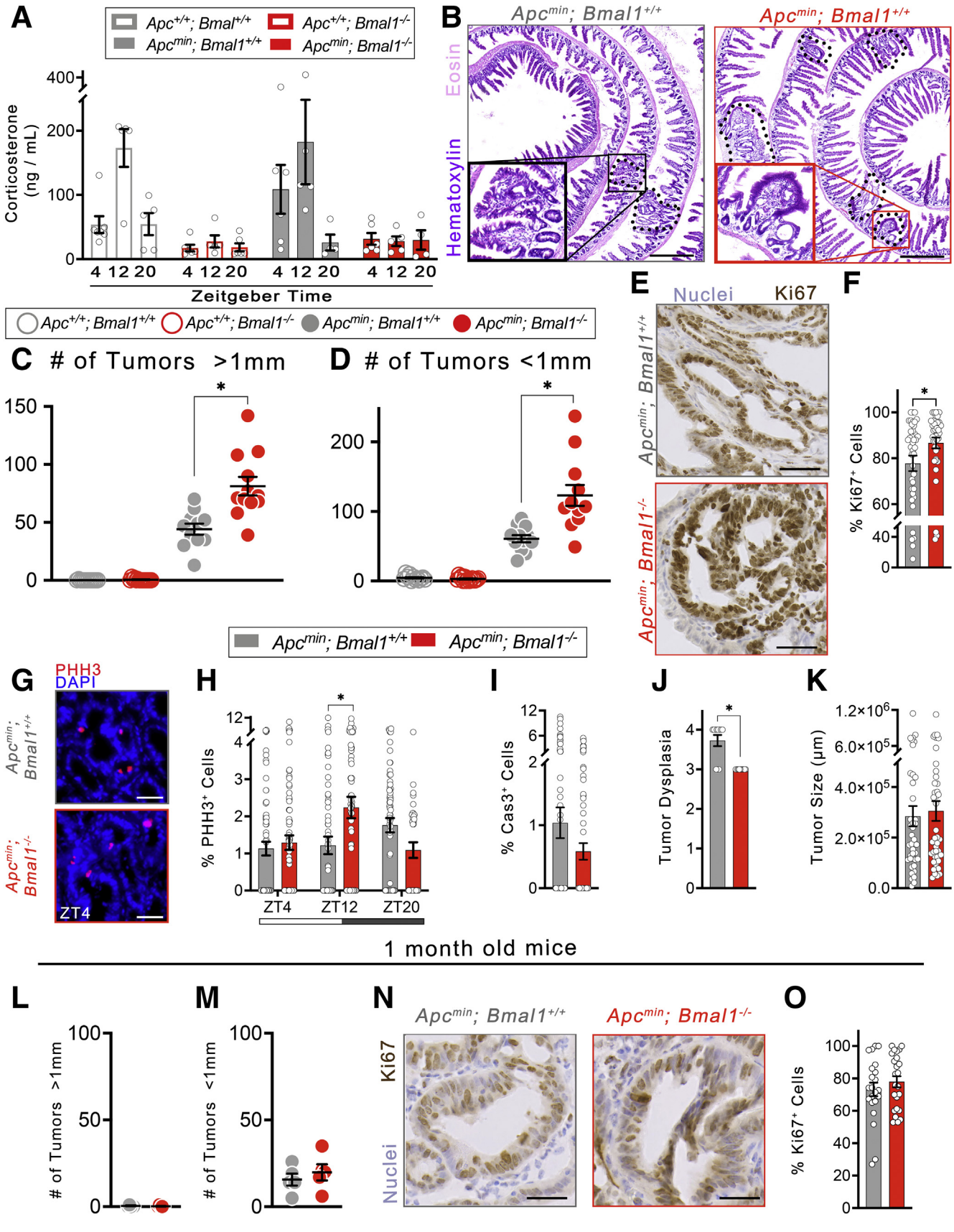
A
Apc+/+; Bmal+/+
Apc+/+; Bmal1-/-
Apcmin; Bmal1+/+
Apcmin; Bmal1-/-
Corticosterone (ng / mL)
400
200
100
0
4 12 20 4 12 20 4 12 20 4 12 20
Zeitgeber Time
B
Apcmin; Bmal1+/+
Apcmin; Bmal1+/+
Eosin
Hematoxylin
C # of Tumors >1mm
D # of Tumors <1mm
150
100
50
0
200
100
0
*
E
Nuclei
Ki67
Apcmin; Bmal1+/+
Apcmin; Bmal1-/-
F
% Ki67+ Cells
100
80
60
40
0
G
PHH3
DAPI
Apcmin; Bmal1+/+
Apcmin; Bmal1-/-
ZT4
H
% PHH3+ Cells
12
4
3
2
1
0
ZT4
ZT12
ZT20
I
% Cas3+ Cells
12
6
2
1
0
J
Tumor Dysplasia
4
3
2
1
0
K
Tumor Size (µm)
1.2×10^6
6.0×10^5
4.0×10^5
2.0×10^5
0.0
1 month old mice
L
# of Tumors >1mm
100
50
0
M
# of Tumors <1mm
100
50
0
N
Apcmin; Bmal1+/+
Apcmin; Bmal1-/-
Ki67
Nuclei
O
% Ki67+ Cells
100
80
60
40
20
0

Epithelial Self-Renewal Is Regulated by Bmal1

We next compared changes in gene expression between genotypes over the full 24-hour period. There were 111 genes changed, either up-regulated or down-regulated, when comparing *Bmal1*$^{+/+}$ controls and *Bmal1*$^{-/-}$ mutant organoids (Supplementary Table 2). *Bmal1*$^{-/-}$ organoids showed 67 genes increased in expression (Figure 5*A*, Supplementary Table 2), which included inflammatory markers such as *Reg3a*, *Reg3b*, and *Cntf*, indicative of a stress/inflammatory state.[60] Compared with non-transformed wild-type controls, *Apc*^{min} tumor organoids up-regulate genes involved in proliferation, Wnt signaling, and inflammation, but down-regulate genes involved in metabolism and clock activity (Supplementary Tables 2 and 3). This is consistent with the role of *Apc* as a Wnt pathway repressor. *Apc*^{min} + *Bmal1*$^{-/-}$ organoids up-regulate or down-regulate 2398 genes when compared with *Apc*^{min} organoids (Supplementary Table 2). Of note, Wnt target genes and apoptosis genes were down-regulated in the absence of *Bmal1*, but Hippo target genes, as well as many genes involved in proliferation, were up-regulated (Figure 5*B* and *C*, Supplementary Tables 2 and 3). To confirm the increase in Hippo signaling, we performed Gene Set Enrichment Analysis (GSEA)[61] using a gene set containing genes previously found to be regulated by the Hippo pathway transducers *Yap* and *Taz* in the intestinal epithelium.[43] Yes-associated protein 1 (Yap)–up-regulated genes are enriched in *Apc*^{min}; *Bmal1*$^{-/-}$ organoids (Figure 5*D*), consistent with the role of the Hippo pathway in promoting cell survival.

A tumor-initiating cell's ability to generate a tumor is thought to be related to self-renewal, a property of adult tissue stem cells.[62] Both crypt progenitors and/or ISCs contribute to tumor initiation,[37,63] and self-renewal can be tested in organoid culture, where single Lgr5+ ISCs[64] or Lgr5- intestinal precursors can generate organoids.[65] We developed an organoid assay to measure self-renewal directly, by directly subcloning 1 single organoid dissociated into single cells and measuring secondary clone number and crypt formation in the resulting subclones (Figure 5*E*). This showed self-renewal at the level of a single organoid, spawned from 1 stem cell, rather than from a population whose secondary organoid numbers are an average that obscures individual organoid self-renewal. Based on our results, we predicted that *Bmal1*$^{-/-}$ epithelial cells, which have higher tumor initiation (Figure 1*B*–*D*), would have increased self-renewal. Indeed, nontransformed *Bmal1*$^{-/-}$ organoids produced twice as many secondary organoids from a single organoid (Figure 5*F* and *G*), and these secondary organoids had many more crypts present, further indicating increased self-renewal (Figure 5*H*). Transformed *Apc*^{min} + *Bmal1*$^{-/-}$ organoids also showed higher self-renewal ability (Figure 5*I*–*K*), suggesting that both non-transformed and transformed *Bmal1*$^{-/-}$ epithelial cells have an organoid initiation advantage. To test the role of the Hippo pathway, we treated *Apc*^{min} + *Bmal1*$^{-/-}$ organoids with small-molecule inhibitors of Yap and its binding partner Tead.[55,66] Yap inhibition reduces the expression of *Ereg*, a critical Yap/Taz target gene that regulates ISC growth[43] (Figure 5*L*), but does not affect the expression of the Wnt pathway target *Axin2* (not shown). Treatment of *Apc*^{min}; *Bmal1*$^{-/-}$ organoids with the Yap inhibitor abolished their increased self-renewal (Figure 5*M*), and treatment with a Tead4-specific inhibitor showed a similar effect (not shown). Overall, these results suggest that *Bmal1* suppresses a Hippo-dependent, self-renewal pathway in the intestinal epithelium, and in its absence the self-renewal of ISCs or tumor-initiating clones is increased.

Epithelial Bmal1 *Contributes to Increased Tumor Initiation*

To what extent does the epithelium play a role in the increased tumor initiation of *Bmal1*$^{-/-}$ mutants in vivo? To address this question, we crossed *Apc*^{min} mice with *Villin*-Cre[67] and *Bmal1*$^{flox/flox}$ mice[68] to delete exon 8—the DNA transactivation domain—thereby conditionally abolishing *Bmal1* and thus circadian transcriptional activity only in the epithelial cells in the *Apc*^{min} background (Figure 6*A*). Three-month-old *Apc*^{min} conditional knockout (cKO) control mice (*Apc*$^{min/+}$; *Bmal1*$^{flox/flox}$) and *Apc*^{min} + *Bmal1* cKO mice (*Apc*$^{min/+}$; *Vil*$^{cre/+}$; *Bmal1*$^{flox/flox}$) were tested, showing that the *Apc*^{min} + *Bmal1* cKO mice had an equal number of large tumors, but 2-fold higher small tumors (Figure 6*B* and *C*). This shows that loss of *Bmal1* in the epithelium partially recapitulates the full mutant phenotype.

Figure 1. (*See previous page*). Loss of *Bmal1* increases tumor initiation in the intestine. (*A*) *Apc*$^{+/+}$;*Bmal1*$^{+/+}$ (wild-type controls, n = 17), *Apc*$^{+/+}$;*Bmal1*$^{-/-}$ (*Bmal1*$^{-/-}$ mutants, n = 20), *Apc*^{min};*Bmal1*$^{+/+}$ (*Apc*^{min} controls, n = 17), and *Apc*^{min};*Bmal1*$^{-/-}$ (*Apc*^{min} + *Bmal1*$^{-/-}$ mutants, n = 18) were tested. Blood serum corticosterone levels were higher and diurnal in control and *Apc*^{min} control genotypes, but invariant and low in both *Bmal1*$^{-/-}$ genotypes (ANOVA, $f_{(6,\ 52)} = 2.766$; $P = .0208$). (*B*) Representative images showing tumors in *Apc*^{min} controls (*left*) and *Apc*^{min} + *Bmal1*$^{-/-}$ mutants (*right*). *Scale bar*: 500 μm. (*C* and *D*) Tumors larger than 1 mm in diameter were increased significantly in *Apc*^{min} + *Bmal1*$^{-/-}$ (ANOVA, $f_{(3,\ 46)} = 80.56$; $P < .0001$), as well as the smaller (<1 mm) tumors (ANOVA, $f_{(3,\ 47)} = 57.41$; $P < .0001$). (*E* and *F*) Cell proliferation (Ki67+) is more intense and higher in *Apc*^{min} + *Bmal1*$^{-/-}$ tumors (*t* test, $P = .0338$). *Scale bar*: 50 μm. (*G* and *H*) Mitotic cells (PHH3+) are increased in *Apc*^{min} + *Bmal1*$^{-/-}$ tumors (ANOVA, $f_{(2,\ 390)} = 5.936$; $P = .0029$). *Scale bar*: 25 μm. (*I*) No significant difference in cell death (caspase 3 [Cas3]$^{+}$) was observed in the tumors. (*J*) *Apc*^{min} + *Bmal1*$^{-/-}$ tumors show reduced tumor dysplasia (*t* test, $P <$ .0001). (*K*) Tumor size in *Apc*^{min} + *Bmal1*$^{-/-}$ was not affected. (*L* and *M*) The number of tumors was equivalent in 1-month-old *Apc*^{min} controls compared with *Apc*^{min} + *Bmal1*$^{-/-}$ mice. (*N* and *O*) Proliferation marker (Ki67) was more intense in the tumors but the percentage of Ki67+ cells was equivalent. *Scale bar*: 50 μm. Histologic quantification shown for n = 10 crypts/regions per animal, and n $\geq$ 3 animals per condition. All error bars represent SEM. Zeitgeber Time (ZT) is indicated, where ZT 0–12 is the light phase and ZT 12–24 is the dark phase of a photoperiod cycle. DAPI, 4′,6-diamidino-2-phenylindole.

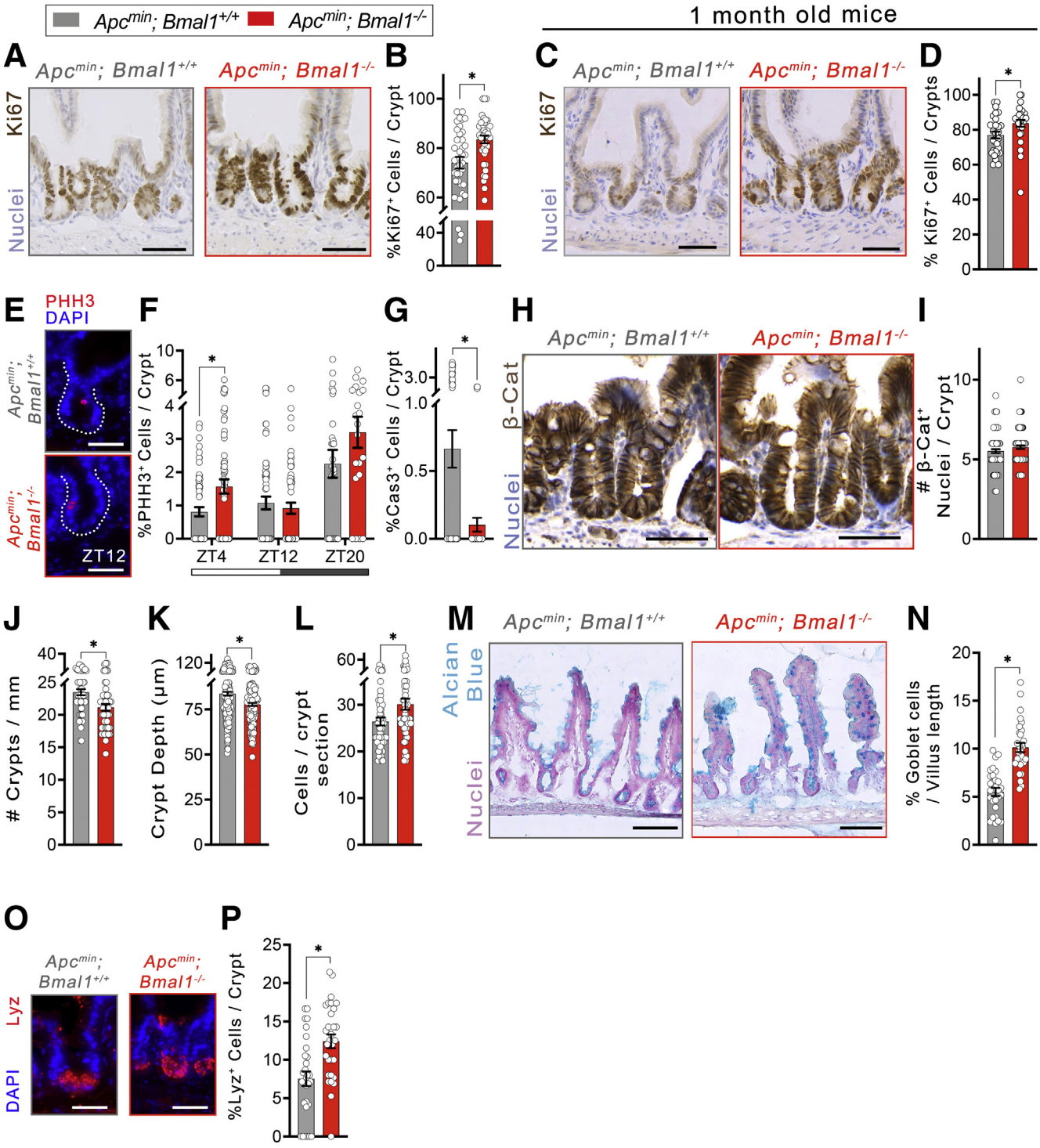

Figure 2. Loss of *Bmal1* alters tissue homeostasis. (*A* and *B*) Ki67+ expression was more intense and increased Ki67+ cells were present in Apc^{min} + $Bmal1^{-/-}$ crypts at 3 months of age (*t* test, $P = .0012$). *Scale bar*: 50 μm. (*C* and *D*) Earlier, at 1 month, these proliferation differences also were present, suggesting the tissue of $Bmal1^{-/-}$ mutants is primed for increased tumor initiation before tumors double in number (*t* test, $P = .0166$). *Scale bar*: 50 μm. (*E* and *F*) Slightly increased mitosis ($PHH3^{+}$) was observed in Apc^{min} + *Bmal1* mutant crypts at 3 months (ANOVA $f_{(2, 218)} = 3.386$; $P = .0352$). *Scale bar*: 25 μm. (*G*) Reduced apoptosis (caspase 3 [$Cas3]^{+}$) was observed in Apc^{min} + $Bmal1^{-/-}$ crypts (*t* test, $P = .031$). (*H* and *I*) β-cat positive (activated) nuclei were equal, suggesting that Wnt signaling was equally active in Apc^{min} control (*left*) and Apc^{min} + *Bmal1* mutant (*right*) crypts. *Scale bar*: 50 μm. (*J*) Slightly fewer crypts were noted in Apc^{min} + *Bmal1* mutant animals (*t* test, $P = .0013$). (*K*) Slightly reduced crypt depth was noted in the Apc^{min} + *Bmal1* mutant (*t* test, $P < .0001$). (*L*) Slightly more cells also were found in the same (*t* test, $P = .0123$). (*M* and *N*) The number of secretory goblet cells (Alcian Blue) was higher in the Apc^{min} + *Bmal1* mutant animals as well (*t* test, $P < .0001$). *Scale bar*: 100 μm. (*O* and *P*) Significantly more Paneth cells (lysozyme [Lyz]+) were present in Apc^{min} + *Bmal1* mutant animals (*t* test, $P = .0005$). *Scale bar*: 25 μm. Histologic quantification is shown for n = 10 crypts/regions per animal, and n ≥ 3 animals per condition. All error bars represent SEM. β-Cat, β-catenin; DAPI, 4′,6-diamidino-2-phenylindole.

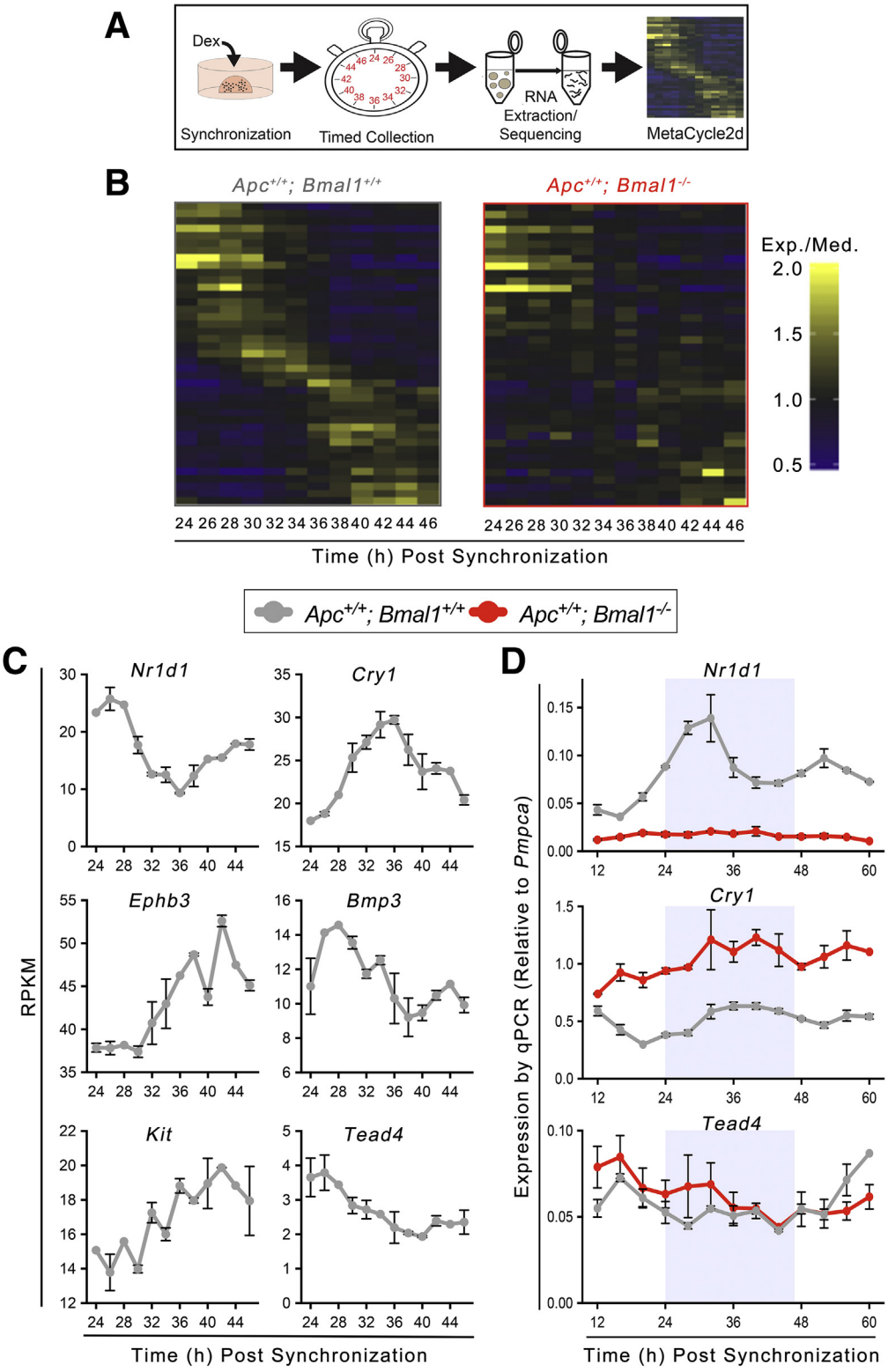

Figure 3. Analysis of circadian transcription in the crypt epithelium. (*A*) Organoids derived from the ileum of control and *Bmal1* mutant mice were passaged, then synchronized using dexamethasone. RNA was isolated at 2-hour intervals from 24 to 48 hours in free-running conditions. RNA sequencing data were analyzed for circadian rhythmicity using MetaCycle's meta2D function (n = 2 organoid lines/genotype). (*B*) Heat maps showing median-normalized gene expression (Exp./Med.) ordered by MetaCycle phase to depict all significant circadian genes found in controls (41 genes). The same genes were arrhythmic in *Bmal1*$^{-/-}$ mutants. (*C*) Graphs showing cycling genes from the RNA sequencing: *Nr1d1* (q = 0.00039), *Cry1* (q = 0.00039), *Bmp3* (q = 0.057), *Ephb3* (q = 0.0084), *Kit* (q = 0.067), and *Tead4* (q = 0.0098). Mutants do not show circadian rhythms in any genes (q > 0.1). (*D*) Two-day quantitative polymerase chain reaction (qPCR) was used to validate the results of the RNA sequencing. *Pmpca* was used as the endogenous control, the gene that was determined by RNA sequencing to be stable across 24 hours in all genotypes. All error bars represent SEM. Dex, Dexamethasone; RPKM, Reads Per Kilobase of transcript, per Million mapped reads.

Are there other factors that drive tumorigenesis in the *Bmal1*$^{-/-}$ mutant? The circadian clock regulates many different rhythms in physiology, including daily cycles of metabolism and the endocrine and immune systems.[4,12] Inflammation is an important driving factor in colorectal tumorigenesis,[39] and the circadian clock also recently was shown to regulate inflammation in the intestine.[69,70] We therefore asked whether *Apc*^{min} + *Bmal1*$^{-/-}$ mice have

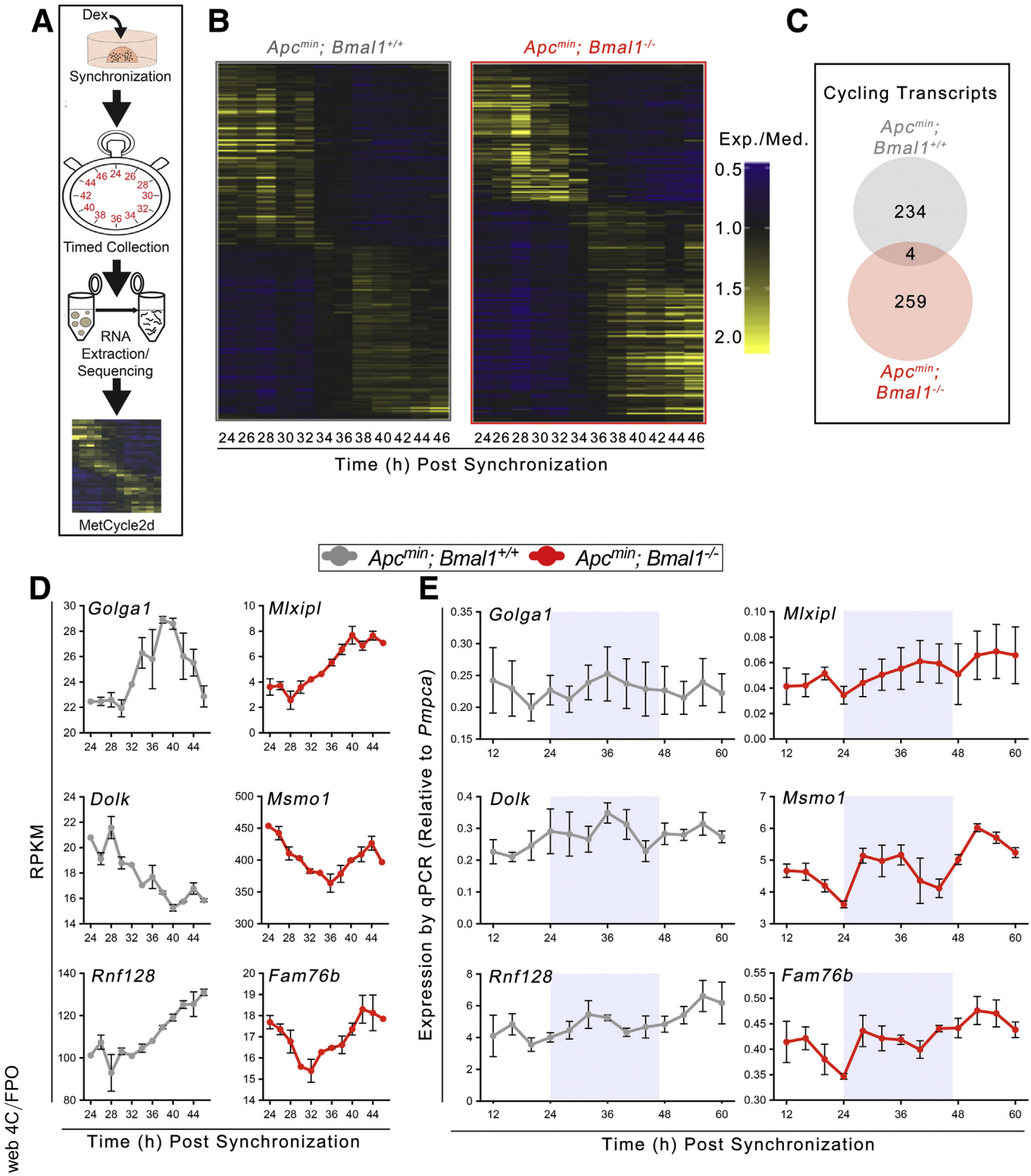

Figure 4. Analysis of circadian transcription in the tumor epithelium. (*A*) Tumor organoids were derived from *Apc*^{min} and *Apc*^{min} + *Bmal1*$^{-/-}$ mice, and then RNA was analyzed by sequencing as shown in Figure 2 (n = 2 organoid lines/genotype). (*B*) Heat maps median-normalized gene expression (Exp./Med.) ordered by MetaCycle phase show all rhythmic genes. (*C*) Venn diagram showing that there is nearly no overlap between rhythmic transcripts identified from wild-type and mutant samples. (*D*) Graphs of the RNA sequencing of the top 3 genes from each genotype: *Golga1* ($q = 0.015$), *Dolk* ($q = 0.015$), *Rnf128* ($q = 0.015$), *Mlxipl* ($q = 0.0053$), *Msmo1* ($q = 0.0053$), and *Fam76b* ($q = 0.0055$). (*E*) Validation test using 2-day quantitative polymerase chain reaction (qPCR) indicated that only *Rnf128* (ANOVA, $f_{(12,24)} = 1.378$; $P = .2427$) and *Msmo1* (ANOVA $f_{(12, 26)} = 4.613$; $P = .0005$) show self-sustaining rhythms. All error bars represent SEM. Dex, Dexamethasone; RPKM, Reads Per Kilobase of transcript, per Million mapped reads.

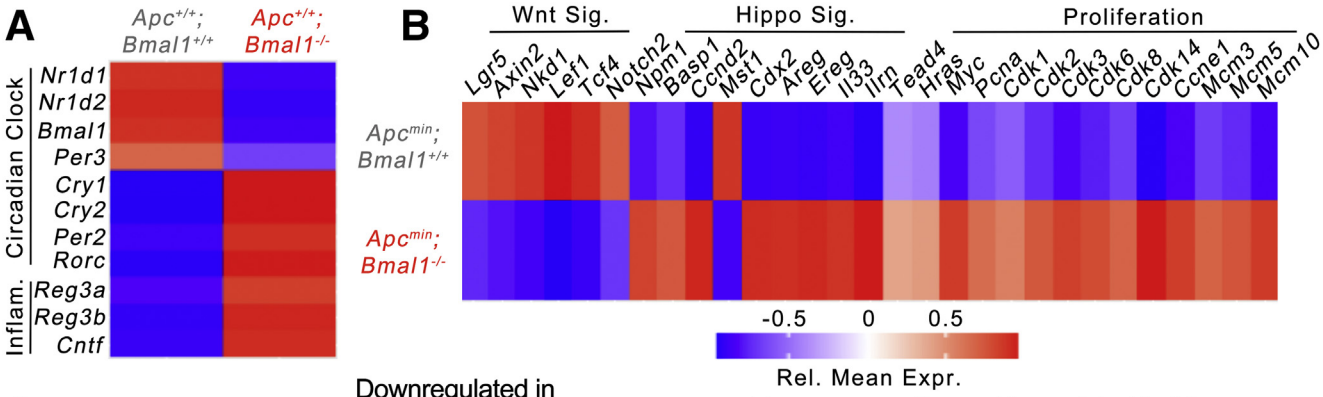
A
Apc+/+; Bmal1+/+
Apc+/+; Bmal1-/-
Circadian Clock
Nr1d1
Nr1d2
Bmal1
Per3
Cry1
Cry2
Per2
Rorc
Inflam.
Reg3a
Reg3b
Cntf
B
Wnt Sig.
Hippo Sig.
Proliferation
Lgr5 Axin2 Nkd1 Lef1 Tcf4 Notch2 Npm1 Basp1 Ccnd2 Msf1 Cdx2 Areg Ereg Il33 Ilrn Tead4 Hras Myc Pcna Cdk1 Cdk2 Cdk3 Cdk6 Cdk8 Cdk14 Ccne1 Mcm3 Mcm5 Mcm10
Apcmin; Bmal1+/+
Apcmin; Bmal1-/-
-0.5 0 0.5
Rel. Mean Expr.

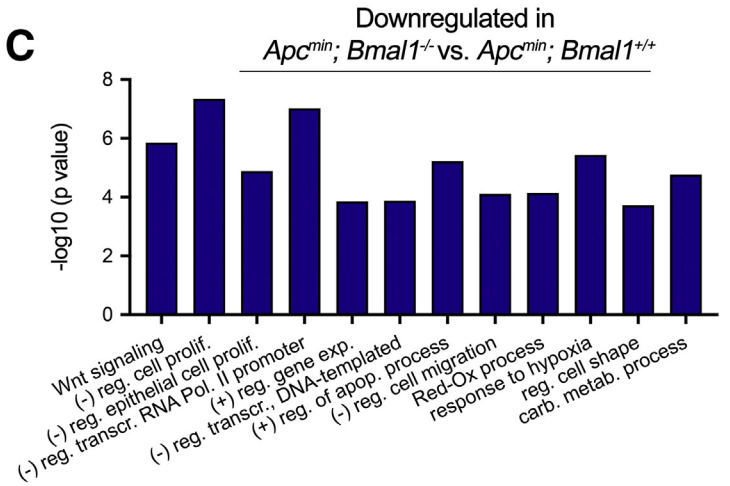
C
Downregulated in
Apcmin; Bmal1-/- vs. Apcmin; Bmal1+/+
-log10 (p value)
0 2 4 6 8
Wnt signaling
(-) reg. cell prolif.
(-) reg. epithelial cell prolif.
(-) reg. transcr. RNA Pol. II promoter
(+) reg. gene exp.
(-) reg. transcr., DNA-templated
(+) reg. of apop. process
(-) reg. cell migration
Red-Ox process
response to hypoxia
reg. cell shape
carb. metab. process

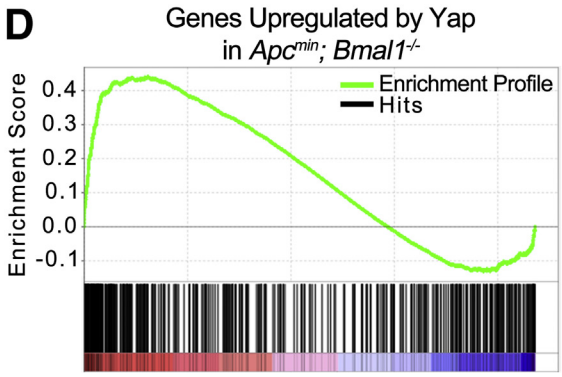
D
Genes Upregulated by Yap
in Apcmin; Bmal1-/-
Enrichment Score
0.4 0.3 0.2 0.1 0.0 -0.1
Enrichment Profile
Hits

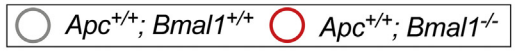
Apc+/+; Bmal1+/+
Apc+/+; Bmal1-/-

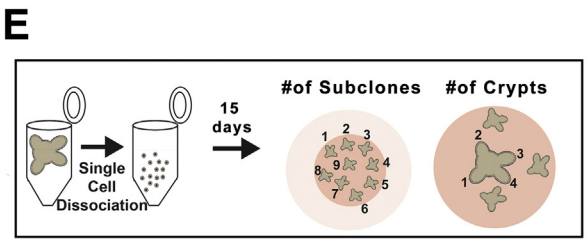
E
Single Cell Dissociation
15 days
#of Subclones
#of Crypts

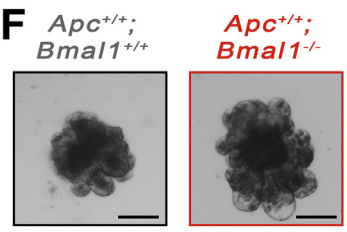
F
Apc+/+; Bmal1+/+
Apc+/+; Bmal1-/-

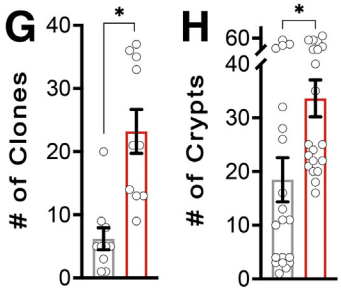
G
# of Clones
0 10 20 30 40
*
H
# of Crypts
0 10 20 30 40 60
*


Apcmin; Bmal1+/+
Apcmin; Bmal1-/-

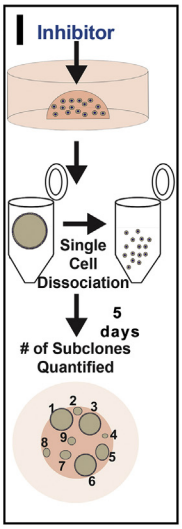
I
Inhibitor
Single Cell Dissociation
5 days
# of Subclones Quantified

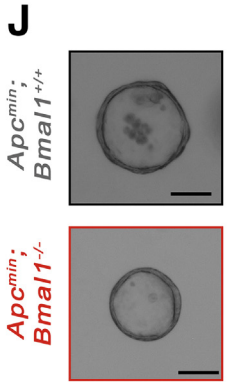
J
Apcmin; Bmal1+/+
Apcmin; Bmal1-/-

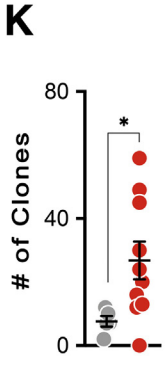
K
# of Clones
0 40 80
*

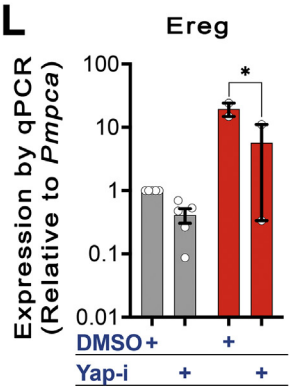
L
Ereg
Expression by qPCR
(Relative to Pmpca)
0.01 0.1 1 10 100
*
DMSO + +
Yap-i + +

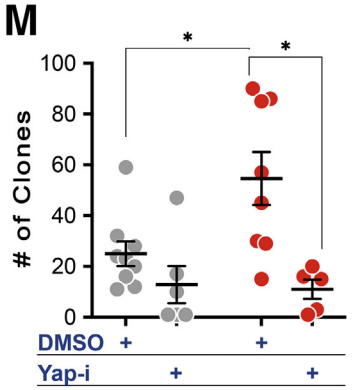
M
# of Clones
0 20 40 60 80 100
* *
DMSO + +
Yap-i + +

increased inflammation, which together with the epithelium could contribute to tumor initiation. Blood was analyzed from the full-body KO and cKO mice, and tested for proinflammatory cytokines. Analysis of a panel of cytokines showed that *Apc*^{min} + *Bmal1*$^{-/-}$ mice have increased levels of Tumor Necrosis Factor (Tnf) (Figure 6*D*), a clock-regulated proinflammatory cytokine.[46] However, *Apc*^{min} + *Bmal1* cKO mice did not show this increase in Tnf. To test whether local inflammation surrounding the epithelium is higher, CD45^{+} blood cell infiltration into tumors was quantified. cKO controls, *Apc*^{min} + *Bmal1* cKO, and *Apc*^{min} + *Bmal1*$^{+/+}$ tumors, have equivalent lower numbers of CD45^{+} cells, while *Apc*^{min} + *Bmal1*$^{-/-}$ tumors have significantly higher CD45+ numbers, indicating a proinflammatory state (Figure 6*E* and *F*). We conclude that global circadian disruption in *Apc*^{min} + *Bmal1*$^{-/-}$ mice drives a protumorigenic inflammatory phenotype that is not present in the *Apc*^{min} + *Bmal1* cKO.

Yap Activity Is Increased in Bmal1 *Mutant Tumors*

The Hippo signaling transducer, *Yap*, is required for tumorigenesis in the *Apc*^{min} colorectal cancer model.[43] We therefore probed *Apc*^{min} controls and *Apc*^{min} + *Bmal1*$^{-/-}$ with an antibody marking Yap to determine if Hippo signaling is perturbed when *Bmal1* is absent. *Apc*^{min} + *Bmal1*$^{-/-}$ epithelial tumors have higher levels of Yap, and the signal shows an active/nuclear localization compared with *Apc*^{min} controls (Figure 7*A* and *B*). Protein was extracted from the tumors of *Apc*^{min} control and *Apc*^{min} + *Bmal1*$^{-/-}$ mice and analyzed by Western blot to further test Hippo activity. Both total Yap and activated Yap (nonphosphorylated S127) are higher in *Apc*^{min} + *Bmal1*$^{-/-}$ tumors (Figure 7*C*). This shows that Yap expression and activity is higher in *Bmal1* mutant tumors consistent with the Yap signature of *Apc*^{min} + *Bmal1*$^{-/-}$ tumor organoids (Figure 5*D*).

To address whether this Yap increase is owing to epithelial *Bmal1* function, *Apc*^{min} cKO control mice and *Apc*^{min} + *Bmal1* cKO mice were tested for markers of the Wnt and Hippo pathways. *Apc*^{min} + *Bmal1* cKO mice have increased levels of Yap localized in the nucleus (Figure 7*D* and *E*) similar to those in *Apc*^{min} + *Bmal1*$^{-/-}$ mutants. Expression of the Hippo pathway component *Tead4*[55] also was increased in *Apc*^{min} + *Bmal1* cKO tumors (Figure 7*F* and *G*). We further probed for the Wnt target, *Axin2*, and the Yap target, *Ereg*, in the *Apc*^{min} + *Bmal1* cKO tumors. The *Bmal1* cKO tumors have lower Wnt but higher Hippo pathway activity (Figure 7*H* and *I*). The results of the *Axin2*/*Ereg* analysis mirror those of the *Lgr5*/*Tead4* expression almost exactly, both indicating that the *Bmal1* tumors have higher Hippo signaling at the expense of Wnt. Of note, Wnt markers (*Lgr5* and *Axin2*) and Hippo markers (*Tead4* and *Ereg*) are enriched in separate cells, suggesting these reflect changes in the tumor cell population. Together, these data show *Bmal1* cKO tumors have lower Wnt but higher Hippo activity, consistent with the *Bmal1*-dependent transcriptional program in *Apc*^{min} + *Bmal1*$^{-/-}$ organoids (Figure 4*B*–*D*). We conclude that *Bmal1* negatively regulates the Hippo pathway in the tumor epithelium and, in its absence, these display higher Hippo activity.

In Vivo Tumors Have Weak Circadian Rhythms

Because tumor organoids do not show rhythmic circadian clock transcription in vitro (Figure 4), we asked whether circadian clock disruption is a general feature of intestinal tumors. We re-examined *Apc*^{min} control mice, housed under normal photoperiod, to determine whether heterogeneity in clock activity or Wnt/Hippo signaling is present in the different tumors initiated. Individual tumors from a cohort of mice over a 24-hour timeline were microdissected (n = 30 mice, 5 per time point), and compared with adjacent nontransformed tissue for gene expression (n = 180 tumor/tissue pairs, n = 30 per time point). *Apc*^{min} tumors showed lower expression of the clock genes *Nr1d1*, *Bmal1*, and *Per2* than the surrounding

Figure 5. (*See previous page*). Epithelial self-renewal is regulated by *Bmal1*. (*A*) Heat map showing 24-hour fold change in relative mean expression of *Bmal1*$^{-/-}$ organoids compared with control organoids. Circadian clock genes were down-regulated, and inflammation markers were up-regulated in Bmal1 mutant organoids compared with controls. (*B*) Heat map showing 24-hour fold change in relative mean expression of *Apc*^{min} + *Bmal1*$^{-/-}$ organoids compared with *Apc*^{min} control organoids. Wnt pathway targets were down-regulated, whereas Hippo pathway targets were up-regulated. Cell proliferation genes also showed an increase in *Apc*^{min} + *Bmal1*$^{-/-}$. (*C*) GO (Gene Ontology) analysis of pathways down-regulated by *Apc*^{min} + *Bmal1* mutant tumor organoids, relative to *Apc*^{min} controls. Wnt signaling was decreased, whereas cell proliferation was increased in *Bmal1* mutants, together with changes in transcriptional regulation. A Benjamini cut-off value of 0.05 was used for GO analysis. (*D*) *Apc*^{min} + *Bmal1*$^{-/-}$ have up-regulated Yap signaling compared with *Apc*^{min} controls (enrichment score, 0.44; normalized enrichment score, 2.083), nominal *P* value = .000, False Discovery Rate (FDR) *q* value = 0.000, Family Wise Error Rate (FWER) *P* value = .000). (*E*) After derivation, individual organoids from each genotype were dissociated into single cells and plated separately to assess the number of subclones, and the number of crypt buds per subclone. (*F*) Representative images of organoid subclones. *Scale bar*: 100 μm. (*G*) Individual *Bmal1*$^{-/-}$ organoids developed more subclones (*t* test, *P* = .0004), indicating increased self-renewal ability. (*H*) *Bmal1*$^{-/-}$ subclones had more crypt buds, indicating further increased self-renewal of ISCs (*t* test, *P* < . 0075). (*I*) Schematic shows clonal analysis of *Apc*^{min} organoids. (*J*) Representative images of *Apc*^{min} and *Apc*^{min} + *Bmal1*$^{-/-}$ organoid subclones. *Scale bar*: 100 μm. (*K*) *Apc*^{min} + *Bmal1*$^{-/-}$ tumor organoids produce more subclones indicating increased self-renewal (*t* test, *P* = .0444). (*L*) *Apc*^{min} control and *Apc*^{min} + *Bmal1*$^{-/-}$ mutant organoids were treated with Yap inhibitor; dimethyl sulfoxide (DMSO) is the vehicle control. *Apc*^{min} + *Bmal1*$^{-/-}$ organoids showed increased expression of the Yap target gene *Ereg*, which was reduced by Yap inhibitor (ANOVA, $f_{(3,10)} = 19.55$; *P* = .002). (*M*) Organoids were pretreated with Yap inhibitor before subcloning. *Apc*^{min} + *Bmal1*$^{-/-}$ organoids showed increased self-renewal, which was disrupted by pretreatment of Yap inhibitor (ANOVA, $f_{(3,\ 24)} = 7.087$; *P* = .00144). Data show n = 10 clones from 2 to 3 lines for quantifications. All error bars represent SEM. Inflam, Inflammation; qPCR, quantitative polymerase chain reaction; Red-Ox, Reduction-Oxidation; Rel Mean Expr, Relative Mean Expression; Sig, Signalling; Yap-i, Yap-inhibitor.

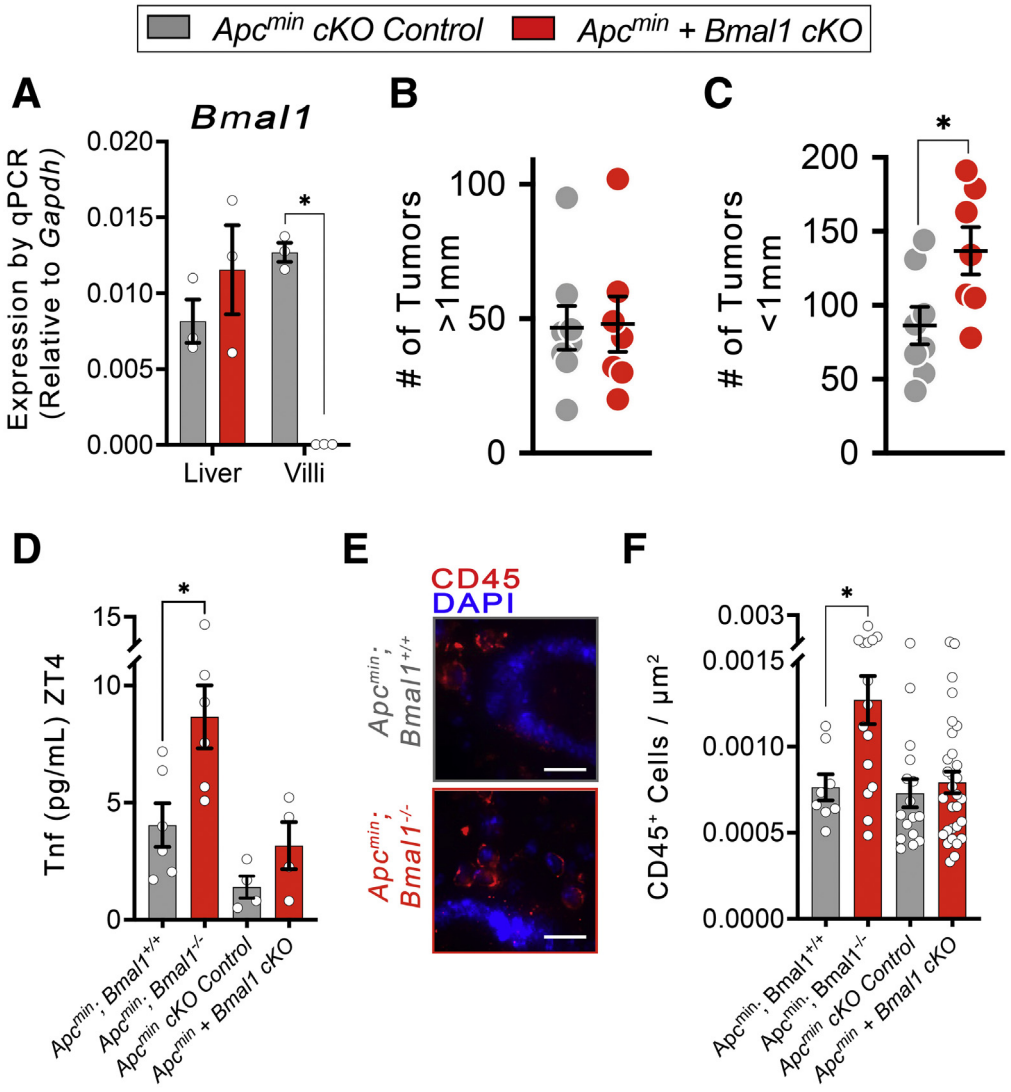

Figure 6. Epithelial *Bmal1* contributes to increased tumor initiation. (*A*) *Bmal1* was expressed in the intestine of controls, but was absent in the intestine of *Bmal1* cKO (*Apc*^{min}; *Vil*$^{Cre/+}$; *Bmal1*$^{fl/fl}$). In the liver, both controls and cKO expressed *Bmal1*, indicating the specific deletion of *Bmal1* from the intestine ($f_{(3,8)} = 11.48$; $P = .0026$; n = 3 per genotype). (*B* and *C*) *Apc*^{min} + *Bmal1 ckO* (n = 7) have an equivalent number of tumors greater than 1 mm, but significantly more tumors smaller than 1 mm, compared with *Apc*^{min} cKO controls (n = 8) (*t* test, $P = .027$). (*D*) Tnf is higher in *Apc*^{min} +_*Bmal1*$^{-/-}$ mutants compared with controls and both of the cKO genotypes (ANOVA, $f_{(3,16)} = 8.42$; $P = .0014$; n = 4–6 mice per genotype). (*E* and *F*) Tumor tissue from *Apc*^{min} + *Bmal1*$^{-/-}$ tumors show an increased number of infiltrating CD45+ blood cells than the other genotypes (ANOVA, $f_{(3,65)} = 6.824$; $P = .005$). Histologic quantification shown for n = 10 regions per animal, and n ≥ 3 animals per condition. *Scale bar*: 10 µm. All error bars represent SEM. DAPI, 4′,6-diamidino-2-phenylindole; qPCR, quantitative polymerase chain reaction; Zeitgeber Time.

web 4C/FPO

nontransformed tissue, and at the population level (average) clearly showed reduced circadian rhythms in vivo (Figure 8*A*–*F*). This expression was heterogenous but nearly all individual tumors showed lower clock gene expression than the surrounding nontransformed tissue. We further tested circadian clock activity in the epithelium by staining for the clock component, *Nr1d1*,[2] in *Apc*^{min} controls and *Apc*^{min} + *Bmal1*$^{-/-}$ mutants. Nr1d1 showed daily changes in its levels and nuclear localization in the normal crypt epithelium of *Apc*^{min} control animals (Figure 8*G* and *H*). *Apc*^{min} + *Bmal1*$^{-/-}$ crypts did not show these daily fluctuations but high Nr1d1 levels at all times examined. In tumors present in the same animals tested, Nr1d1 levels fluctuated in tumors in *Apc*^{min} controls at the same time as nontransformed tissue, and *Apc*^{min} + *Bmal1*$^{-/-}$ had high levels at all times (Figure 8*I* and *J*). Nr1d1 protein in tumors thus showed diurnal rhythms such as the surrounding tissue, corroborating the RNA analysis. Overall, we conclude that weak diurnal rhythms in clock components persist in tumors in vivo.

A circadian regulation of the Wnt pathway was reported previously in organoids,[54] hence we examined Wnt signaling in these same samples. In vivo, the intestine showed daily changes in the Wnt pathway targets *Axin2*,

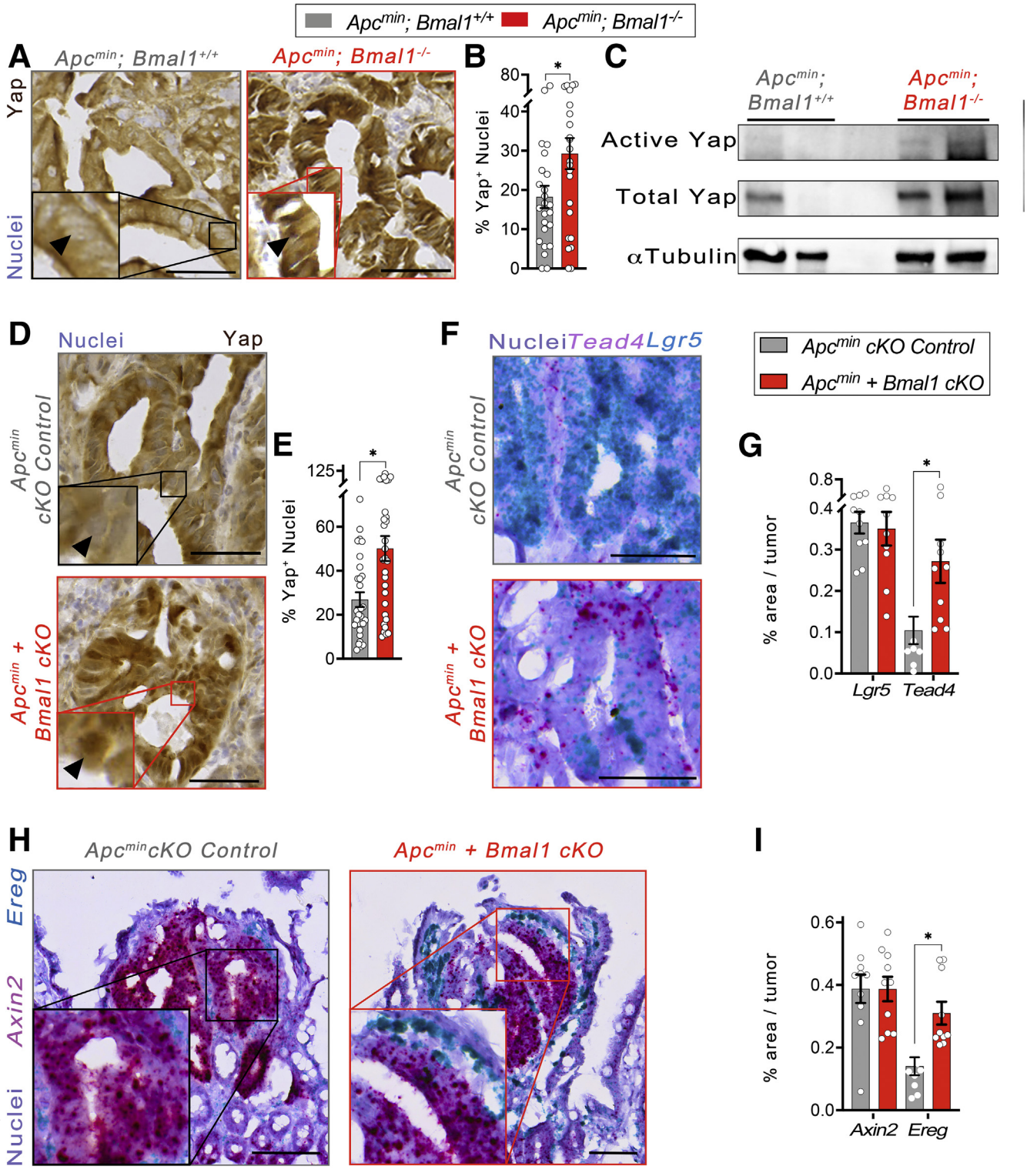

Figure 7. Yap activity is increased in *Bmal1* mutant tumors. (*A* and *B*) Representative images showing increased Yap+ nuclear signal in the cells of Apc^{min} + $Bmal1^{-/-}$ tumors (*arrowheads* show the cell nucleus in inset image). Yap-activated nuclei are present in higher numbers (*t* test, $P = .0186$). *Scale bar*: 50 μm. (*C*) Western blots showing increased levels of total and activated Yap in Apc^{min}; $Bmal1^{-/-}$ mutant tumors. (*D* and *E*) Representative images showing increased Yap+ nuclear signal in the cells of Apc^{min} + *Bmal1* cKO that are present in higher numbers (*t* test, $P = .0009$). *Scale bar*: 50 μm. (*F* and *G*) Control tumors show higher expression of *Lgr5* RNA (blue) while Apc^{min} + *Bmal1* cKO tumors show higher *Tead4* RNA expression (red). The area of *Tead4*+ cells is significantly higher in Apc^{min} + *Bmal1* cKO (ANOVA $f_{(3, 36)} = 9.241$; $P = .0001$). *Scale bar*: 50 μm. (*H* and *I*) Apc^{min} + *Bmal1* cKO tumors show higher levels of the Yap target gene *Ereg* (blue), but lower levels of the Wnt target gene, *Axin2* (red), relative to controls. The area of *Ereg*+ cells is significantly higher (ANOVA $f_{(3, 36)} = 9.422$; $P < .0001$). Histologic quantification shown for n = 5–10 regions per animal, and n ≥ 3 animals per condition. *Scale bar*: 100 μm. All error bars represent SEM.

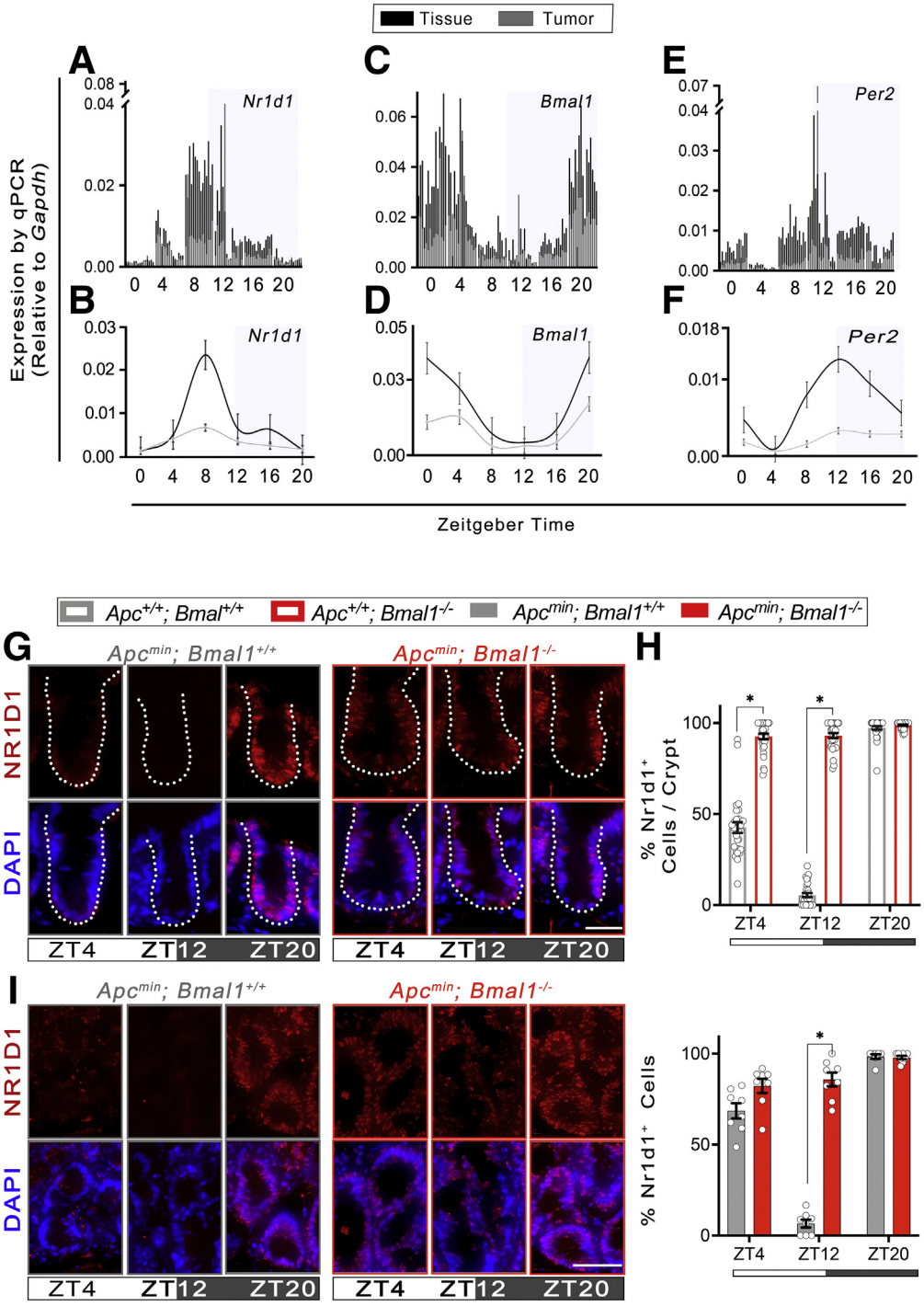

Figure 8. In vivo tumors have weak circadian rhythms. (*A* and *B*) Quantitative reverse-transcription polymerase chain reaction (RT-qPCR) graphs show transcript levels obtained from *Apc*^{min} mice housed under a light dark cycle. Individual tumors were compared directly with their adjacent nontransformed tissue taken from the ileum of the small intestine. Six time points over 24 hours were tested, from 5 mice per time point (n = 30 tumors per time point). Upper graphs shows individual tumor expression, and lower graphs show the average of that time point. *Nr1d1* expression in individual tumors is lower but rhythmic (2-way ANOVA, $f_{(5,\ 168)} = 12.01$; $P < .0001$). (*C* and *D*) *Bmal1* (2-way ANOVA, $f_{(5,\ 168)} = 6.49$; $P < .0001$) also is lower but rhythmic. (*E* and *F*) *Per2* shows lower expression in tumors relative to tissue as well ($f_{(1,\ 168)} = 25.50$; $P < .0001$). (*G* and *H*) Nr1d1 antibody in nontransformed intestinal crypts tested at 3 time points over 24 hours (Zeitgeber Time [ZT]4, 12, 20). *White outlines* shows the crypt border. *Apc*^{min} controls have diurnal changes in Nr1d1 in crypt cells, while *Apc*^{min} + *Bmal1*$^{-/-}$ nontransformed crypts show arrhythmic levels (2-way ANOVA, $f_{(2,\ 116)} = 351.9$; $P < .0001$). (*I* and *J*) Nr1d1 staining in tumors from the same animals. *Apc*^{min} control tumors show diurnal changes, while *Apc*^{min} + *Bmal1*$^{-/-}$ tumors are again arrhythmic (2-way ANOVA, $f_{(2,\ 27)} = 127.4$; $P < .0001$), n = 3 mice per time point. *Scale bar*: 25 μm. Histologic quantification shown for n = 10 crypts/regions and n $\geq$ 3 animals per condition. All error bars represent SEM. DAPI, 4′,6-diamidino-2-phenylindole.

web 4C/FPO

Lgr5, *Ccnd1*, and *cMyc* (Figure 9*A–H*). The Hippo pathway genes *Ereg* and *Tead4* similarly showed diurnal changes (Figure 9*I–L*). Although tumors showed heterogeneity in the expression of Wnt/Hippo target genes, at the population level daily changes were evident, with tumors generally showing increased levels of these cancer and proliferation-related pathways. To further analyze these data, we tested the Pearson correlations of clock genes to Wnt genes in all of these samples. These showed that the normal correlations between the timing of clock and Wnt activity were altered in tumors (Figure 9*M* and *N*). For instance, the negative correlation between *Bmal1* and *Per2* broke down, whereas

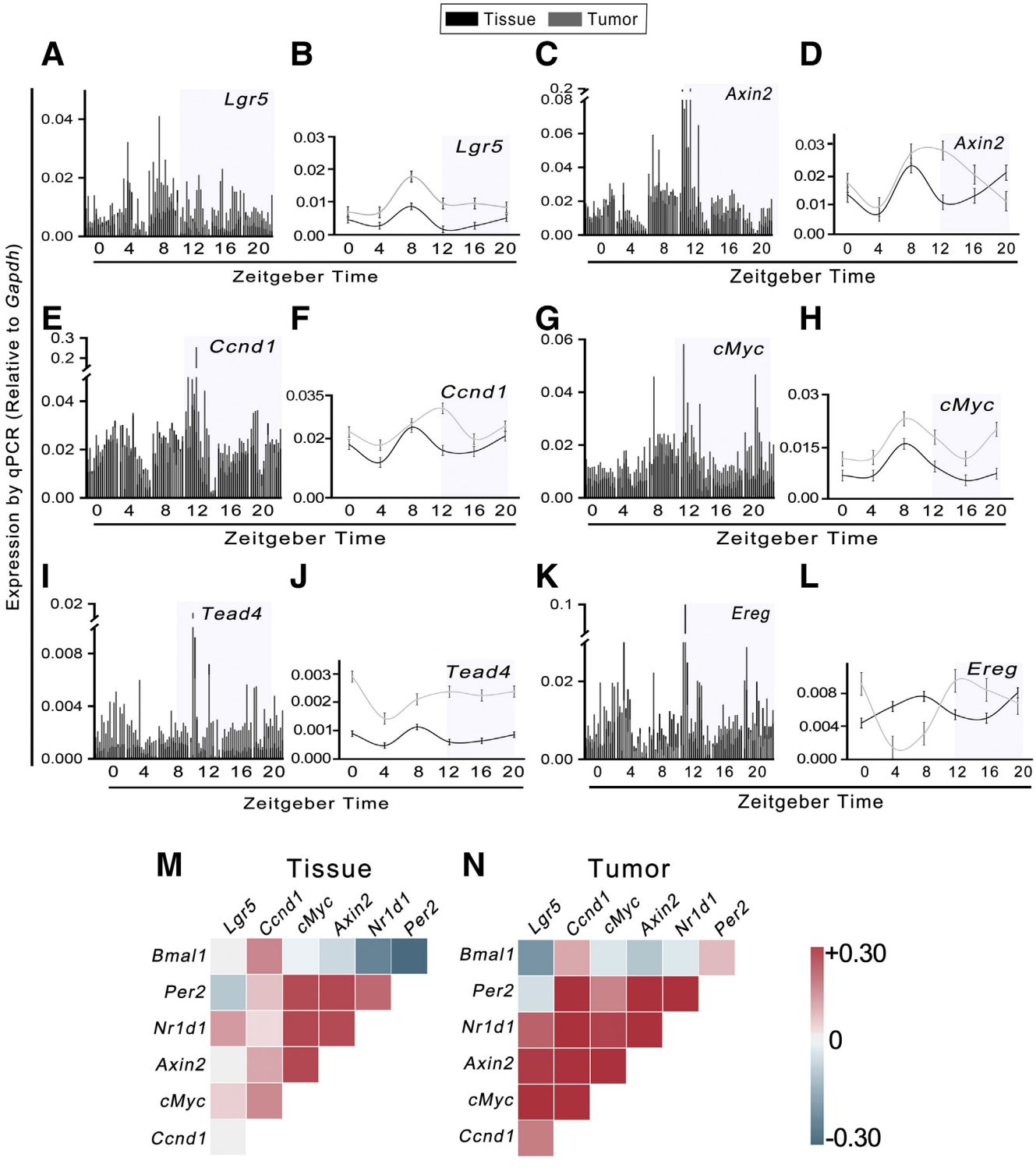

correlations between *Nr1d1* and *Axin2*, *cMyc*, or *Ccnd1* increased. Wnt pathway genes were highest toward the end of the light phase (Zeitgeber Time 8–12), and these rhythms were exacerbated in tumors despite their lower clock activity. These data indicate that individual tumors are heterogenous but all of them had reduced diurnal patterns of circadian clock components that did not correlate to reductions in protumorigenic signaling.

Circadian Rhythm Loss Potentiates Tumor Initiation

Circadian rhythms in mice are entrained by photoperiod, and the behavioral and physiological rhythms that ensue consolidate circadian clock function in tissues throughout the body.[71] Our results thus far show the effects of *Bmal1* loss in tumor initiation; however, it is not clear if this is a feature of disrupted circadian rhythms or noncircadian *Bmal1* functions. To address this, we exposed Apc^{min} mice to constant light levels (LLs) that lead to circadian disruption[72] and quantified tumor incidence at 3 months of age. Wild-type mice did not develop tumors in constant light, but Apc^{min} mice showed a 2-fold increase in both small (<1 mm) and large (>1 mm) tumor initiation in constant light compared with those under normal photoperiod (light dark cycle) (Figure 10*A*–*C*), essentially recapitulating the effects observed in the Apc^{min} + *Bmal1* mutant (Figure 1*C* and *D*). This confirms that disruption of circadian rhythms itself was able to increase tumor initiation in the Apc^{min} background. We further tested Hippo signaling and cell proliferation in the LL circadian-disrupted tumors to see whether the same *Bmal1*-dependent increases were present. Apc^{min} mice exposed to constant light showed an increase in Yap-positive tumor cells, with concentrated staining in the nuclei (Figure 10*D* and *E*) identical to both the full body and conditional *Bmal1* knockout mice (Figure 7*A*, *B*, *D*, and *E*). Ki67 was increased in the crypts (Figure 10*F* and *G*) and tumors of Apc^{min} LL mice (Figure 10*H* and *I*), similar to the $Bmal1^{-/-}$ mutant (Figure 1*E* and *F*). These data show that environmental disruption to circadian entrainment through increased light exposure leads to a Yap-active tumor phenotype that resembles the *Bmal1* loss of function phenotype.

Discussion

The effect of circadian rhythms on tumorigenesis is a long-standing question. Studies have shown that shift workers have a higher cancer incidence,[6,7,9,10] suggesting that circadian rhythm disruption is a risk factor. However, the epidemiologic data are not yet conclusive,[14] and studies using animal models to test how clock genes relate to cancer also have been equivocal.[13] Early reports have indicated that lymphoma was increased in *Per2* mutant mice,[28] and this same strain recently was shown to have increased liver and lung tumors.[30,31] Indeed, *Per2* mutant mice have increased intestinal tumorigenesis when crossed to the Apc^{min} model.[29] However, *Per2* is redundant with its homologs *Per1* and *Per3*, and the circadian clock is active in the *Per2* mutant, which has circadian rhythms present.[2,73] Hence, it is not clear if the increased tumorigenesis resulting from *Per2* loss is owing to its role as a circadian clock gene, or to its nonclock functions.

Using the *Apc* model of colorectal cancer we show that tumor initiation is regulated negatively by the circadian clock. Loss of the nonredundant clock gene, *Bmal1*, in a congenic Apc^{min} mouse strain, and circadian disruption in the Apc^{min} strain effected by constant light, both increased tumor number (Figures 1*B*–*D* and 10*A*–*C*). Conditional deletion of *Bmal1* in the intestine also increased tumor number (Figure 6*B* and *C*), showing that *Bmal1* and/or the epithelial clock specifically played a role in suppressing tumor initiation. These experiments confirmed that circadian rhythm disruption in the epithelium is a causal factor in tumorigenesis. Both $Bmal1^{-/-}$ organoids and Apc^{min} + $Bmal1^{-/-}$ organoids have increased self-renewal (Figure 5*E*–*K*), consistent with the idea that these have an enhanced ability to initiate tumors. Although proliferation was increased, we did not observe that *Bmal1* loss increased tumor size (Figure 1*K*), suggesting that the suppressive effects of *Bmal1* may be more complex than simply driving general tumor growth. These data provide insight into the precise stages of tumorigenesis, in which the circadian clock exerts its effects in this tissue.

Bmal1 loss decreases tumorigenesis in the skin,[49] as does its binding partner *Clock*,[74] whereas its negative regulator *Per2* has the opposite effect in the skin and

Figure 9. (***See previous page***). **Analysis of circadian clock, Wnt and hippo genes in the intestine.** Quantitative reverse-transcription polymerase chain reaction (RT-qPCR) graphs from same samples as shown in Figure 8. The Wnt target genes were as follows: (*A* and *B*) *Lgr5* (2-way ANOVA, $f_{(5,\ 168)} = 2.50$; $P = .033$), (*C* and *D*) *Axin2* (2-way ANOVA, $f_{(5,\ 168)} = 9.24$; $P = .0027$), (*E* and *F*) *Ccnd1* 1-way ANOVA, $f_{(1,\ 168)} = 8.947$; $P = .0032$), and (*G* and *H*) *cMyc* (2-way ANOVA, $f_{1,\ 168)} = 71.98$; $P < .0001$), and were higher in tumors but also had diurnal changes similar to the surrounding tissue. (*I* and *J*) The Hippo component *Tead4* is diurnally rhythmic in the intestine and its tumors (2-way ANOVA, $f_{(11,\ 168)} = 5.125$; $P < .0001$). (*K* and *L*) The Hippo target *Ereg*, is rhythmic in tumors but with a different rhythm than surrounding tissue (2-way ANOVA $f_{(5,\ 168)} = 2.746$; $P = .02$). (*A* and *B*) Pearson correlation showing the relationship between clock genes and Wnt pathway targets in nontransformed intestine (tissue) vs transformed tumors (tumor). Tissue normally shows a negative correlation (dark blue) between *Bmal1* and *Nr1d1*, or *Per2*, and weaker correlation between *Per2* and *Nr1d1* and Wnt target genes (*Axin2*, *cMyc*, and *Ccdn1*). Tumors show loss of negative clock correlations, indicating weakened circadian transcription (where positive and negative regulators are expected to be antiphasic and thus negatively correlated). Increased positive correlation (dark red) between clock targets *Per2* and *Nr1d1* and Wnt target genes was observed in tumors. This indicates clock function was weakened, but daily rhythms in Wnt signaling were present in tumors. Error bars represent SEM.

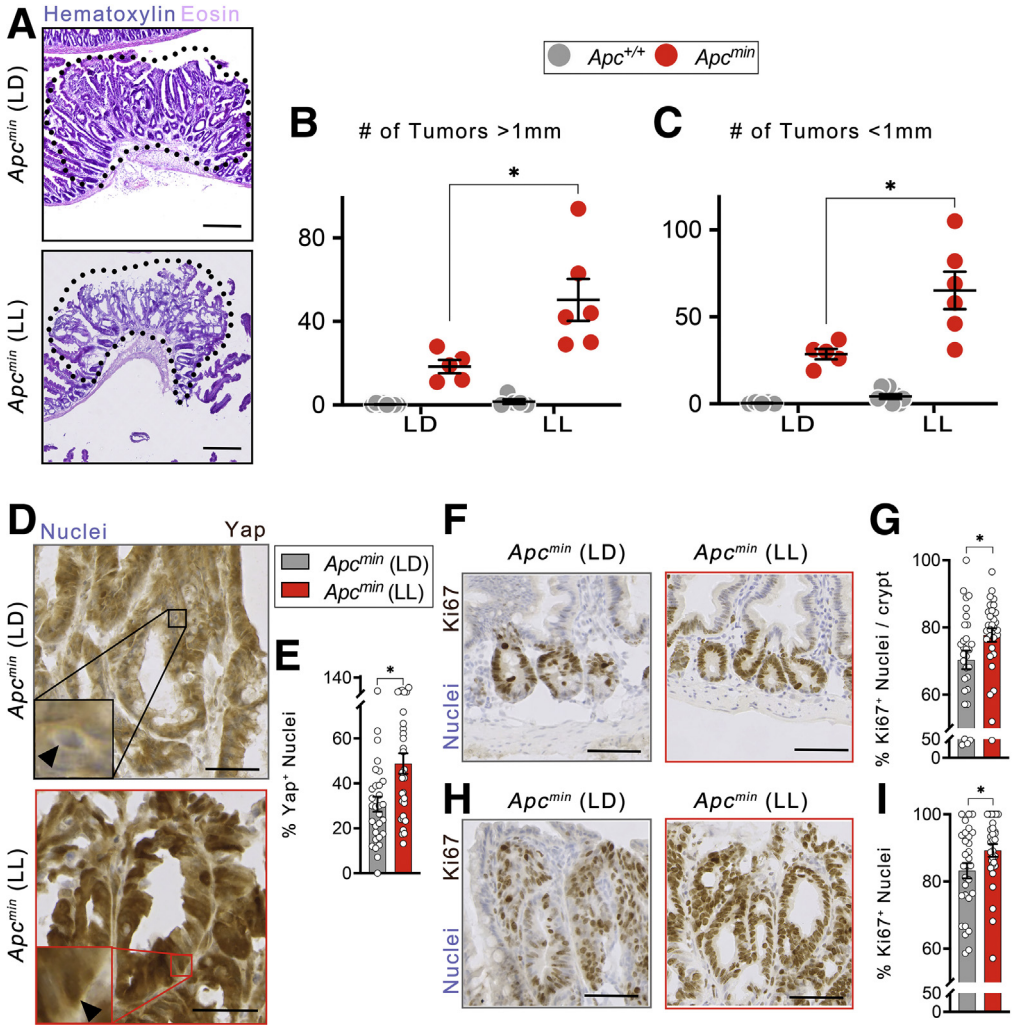

Figure 10. Circadian rhythm loss potentiates tumor initiation. Control mice and *Apc*^{min} mice were tested on a normal 12-hour light/12-hour dark photoperiod (light dark cycle [LD]) vs constant light (LL, 700 Lux) (n = 5–6 per genotype). (*A*) Representative images of tumors found in LD and LL conditions. *Scale bar*: 200 μm. (*B* and *C*) *Apc*^{min} mice in LL develop significantly more large tumors greater than 1 mm in size (ANOVA, $f_{(3,\ 20)} = 20.58$; $P < .0001$), and small tumors of less than 1 mm (ANOVA, $f_{(3,\ 20)} = 28.71$; $P < .0001$) than LD mice, indicating that constant light recapitulates the *Bmal1* mutant phenotype. No tumors were observed in control mice, under both LD and LL conditions, without the *Apc*^{min} allele present. Error bars represent SEM. (*D* and *E*) Representative images of total Yap-stained tumors in *Apc*^{min} (LD) and *Apc*^{min} (LL) show increased Yap+ nuclear signal in the cells of *Apc*^{min} + *Bmal1*$^{-/-}$, which are present in higher numbers (*t* test, $P = .0023$). *Scale bar*: 50 μm. (*F* and *G*) Cell proliferation (Ki67+) is more intense and increased in *Apc*^{min} + *Bmal1*$^{-/-}$ crypts (*t* test $P = .0341$). *Scale bar*: 50 μm. (*H* and *I*) Proliferation also is increased in LL tumors (*t* test $P = .0447$). Histologic quantification shown for n = 10 crypts and n $\geq$ 3 animals per condition. *Scale bar*: 50 μm. All List of Antibodies Used error bars represent SEM.

web 4C/FPO

lung.[30,49] A recent study showed that the clock component *Nr1d1* is a tumor suppressor, whose activation in animal models dramatically reduced cancer.[75] Further studies are needed to determine whether other clock genes have distinct effects on *Apc*^{min} tumor initiation. Our results add to a growing body of literature showing that clock gene disruption leads to cancer in a tissue-specific manner.

Recent studies have shown that tumors in the blood and brain both show and require circadian clock gene function.[76,77] How is this possible? Is each tumorigenic event different, so that some tumors require clock function while others do not? Using circadian wild-type *Apc*^{min} mice, we found that in nearly all intestinal tumors, clock gene rhythms were present but at lower amplitude than the surrounding tissue in vivo (Figure 8*A–F*). Organoids derived from these tumors do not show self-autonomous clock gene transcription rhythms (Figure 4, Supplementary Table 1), showing that these cells lack a circadian oscillator. In vivo, circadian rhythmicity throughout the body is driven by hormones, responses to feeding, or other daily environmental changes experienced by the individual.[52,78] The timing of food availability has been shown to improve circadian clock expression rhythms in tumor cells,[79,80] and can even rescue *Bmal1* loss of function in the liver.[81] This explains how *Apc*^{min} tumor cells mimic the host circadian program in vivo, aligning their expression of circadian clock genes with the normal

physiological rhythms that surround them. This disrupted clock function in tumors is consistent with reports that *cMyc*, increased in Apc^{min} tumors (Figure 9*G* and *H*), inhibits circadian clock transcription.[20,82,83] Indeed, we noted the presence of a cMyc transcriptional signature in Apc^{min} + $Bmal1^{-/-}$ organoids compared with Apc^{min} control (Supplementary Table 5).

Despite their core clock deficiency, Apc^{min} tumor organoids showed 24-hour variation in hundreds of transcripts in vitro, and Apc^{min} + $Bmal1^{-/-}$ tumor organoids showed 24-hour variation in another set of transcripts (Supplementary Table 1). We cannot rule out that some of these 24-hour variations in organoids without a functional clock are false positives caused by genome-wide testing of thousands of genes; nevertheless, the ability of Apc^{min} + $Bmal1^{-/-}$ organoids to show rhythms is a curious phenomenon, previously found to occur in both transcription and metabolism.[84–86] Further experiments are required to classify the nature of these self-sustained oscillations in the absence of the core transcriptional oscillator, and their possible biological implications in organoid culture. In contrast to the tumor epithelium, the nontransformed epithelium shows robust circadian clock activity[87,88] (Figures 8 and 9). Using organoid cultures, we detected 41 self-sustaining rhythmic genes dependent on *Bmal1*[46] (Figure 3). Other studies have detected many more rhythmic genes in the intestine.[89–93] Our RNA sequencing approach differed from these studies in several important respects: (1) testing only the cells of the intestinal epithelium, enriched for crypt precursors present in the first 2 days of organoid cultures; (2) using the $Bmal1^{-/-}$ mutant to distinguish putative core clock targets from rhythmic but non–*Bmal1*-regulated genes; (3) testing circadian gene expression under free-running in vitro conditions to exclude environmental responses (such as photoperiod or feeding) from self-sustaining circadian rhythmicity; and (4) performing high-resolution transcriptomic analysis, which would exclude stochastic noncircadian changes in daily gene expression. We have attempted to follow the guidelines proposed for optimal detection of circadian transcription,[56] and it is apparent that epithelial crypt cells have relatively few rhythmic circadian gene targets. Among these are genes known to be involved in ISC biology, suggesting the circadian clock does indeed regulate aspects of tissue renewal of interest for future study. An important caveat to our analysis is that the gene expression of differentiating cells may obscure circadian expression and therefore our analysis should not be considered exhaustive. Additional tests of specific differentiated cell types in organoids, or longer (ie, 48-hour) timelines, would be informative.

Although our study has focused on the epithelium, other aspects of physiology that are dysregulated in $Bmal1^{-/-}$ mice[51] also may contribute to tumor initiation. The circadian clock is known to regulate many aspects of inflammation,[94] and we report that dysfunction in immune system activity may be an additional factor (Figure 6*D–F*), when the clock is disrupted throughout the body. It has been shown that glucocorticoid rhythms in the body suppress tumor growth.[95] Our analysis, showing lower glucocorticoid levels in $Bmal1^{-/-}$ null genotypes (Figure 1*A*), also supports the additional contribution of disrupted endocrine homeostasis to tumorigenesis in Apc^{min} + $Bmal1^{-/-}$ mice. Both inflammatory and metabolic contributions to tumor growth during circadian disruption will be important to test to distinguish the effects of these contributing factors.[96]

This study reports circadian clock regulation of the Hippo pathway. Apc^{min} + $Bmal1^{-/-}$ organoids show higher Yap/Tead target genes (Figure 5*B* and *D*); Apc^{min} + $Bmal1^{-/-}$ mutant, Apc^{min} Bmal1 intestinal cKO, and Apc^{min} circadian-disrupted (LL) tumors show more Yap activity, and higher *Tead4* and *Ereg* expression (Figures 7 and 10). These changes are associated with concomitant lower levels of Wnt target genes in both organoids and tumors. Wnt pathway activation is the primary cause of Apc^{min}-induced tumorigenesis,[36] but the Hippo pathway is implicated in Apc^{min} tumorigenesis as well.[43] Studies have shown that these pathways may be mutually antagonistic, and consistent with this notion we note that Wnt and Hippo target-expressing cells generally are separate (Figure 7*F–I*). We therefore hypothesize that *Bmal1* negatively regulates the Hippo signaling pathway in the tumor epithelium, and Wnt pathway regulation emerges as a secondary effect. Intestinal regeneration has been proposed to involve the reprogramming of a fetal-like state with high Yap activity.[42,43,97] Crypt cell populations readily dedifferentiate during regeneration,[38] where Yap activity is precisely controlled before the system returns to a primarily Wnt-driven, self-renewal state.[65] An endogenous timekeeper such as the circadian clock would be an ideal system to control the timing of regenerative pathway responses, thereby dictating the time when Wnt and Hippo signaling pathways are engaged during stress and regeneration. This is analogous to the role of the circadian clock in regulating signaling pathways in epidermal stem cells.[49] Understanding the circadian regulation of ISC signaling will help develop cancer-preventing measures, as well as providing insight into the diagnosis and treatment of colorectal cancers in individuals subject to shift work or other forms of circadian disruption.

Methods

Animal Housing and Breeding

Mice were housed on a 12-hour light/12-hour dark cycle with ad libitum food in a barrier facility. Apc^{min} mice (#002020; Jackson Labs, Bar Harbor, ME) were crossed with $Bmal1^{+/-}$ null mutant mice (#009100; Jackson Labs). Progeny were back-crossed for 7 generations to generate a genetically pure strain before experiments began. $Bmal1^{flox/flox}$ mice (#007668; Jackson Labs) were crossed with $Villin^{Cre/+}$ mice (#021504; Jackson Labs), or Apc^{min} mice, then the 2 strains were crossed to obtain the $Apc^{min/+}$; $Bmal1^{flox/flox}$ and $Apc^{min/+}$; $Vil^{Cre/+}$; $Bmal1^{flox/flox}$ for the cKO experiments. Genotyping was performed according to protocols available at Jackson Labs (www.jax.org). All animals were tested for tumor initiation at 1 or 3 months of age. Mice maintained under constant light (LL) were housed in these conditions from 21 days of age to 3 months of age. Light levels were approximately 700 Lux, measured at the

Table 1. List of Antibodies Used

Antibody	Dilution	Assay	Supplier	Product number
Phosphorylated-histone H3 (Ser10)	1:1000	IF	Upstate/Millipore (Oakville, Ontario)	06-570
Cleaved caspase 3	1:200	IF	Cell Signaling Tech (Whitby, Ontario)	9661S
Lysozyme	1:200	IF	Agilent/Dako (Santa Clara, CA)	A0099
Nr1d1	1:250	IF	Abnova (Taipei City, Taiwan)	H00009572 M02
Yap (D841X) XP (R)	1:100 1:1000	DAB WB	Cell Signaling Tech	140745
β-catenin	1:250	DAB	Abcam (Toronto, Ontario)	Ab32572
Ki67	1:100	DAB	Abcam	Ab16667
CD45	1:200	IF	Abcam	ab10558
Nonphosphorylated YAP (Ser127) (E6U8Z) rabbit mAb	1:1000	WB	Cell Signaling Tech	29495S
Tubulin	1:10,000	WB	Sigma	T5168
DK α-rabbit-HRP	1:10,000	WB	Jackson Immunoresearch (West Baltimore Pike, PA)	711-035-152
DK α-mouse-HRP	1:10,000	WB	Jackson Immunoresearch	715-035-150

DAB, 3,3′-diaminobenzidine tetra hydrochloride; DK, Donkey; HRP, horseradish peroxidase; IF, Immuno-Fluoresence; mAb, Monoclonal Antibody; WB, Western Blot; Yap, Yes-associated protein 1.

back of each cage, and all objects were removed so that light fully penetrated throughout each cage. Mice were maintained under Canadian Council for Animal Care guidelines (University of Windsor: AUPP 17-21).

Tissue Collection

All animals were killed using CO_2, followed by cervical dislocation at the times indicated in the figure panels. Intestines then were removed and flushed with ice-cold, phosphate-buffered saline to remove feces. For histologic analysis and tumor counting, the entire length of the small intestine was fixed in 4% paraformaldehyde (PFA) + phosphate-buffered saline (PBS) (Electron Microscopy Sciences, Hatfield, PA) for 2 hours at room temperature. The intestine was subdivided into 4 regions of equal length longitudinally: the proximal intestine closest to the stomach containing duodenum and jejunum, the proximal–medial region containing the jejunum, the distal–medial region containing the jejunum and ileum, and the distal region containing the ileum. In Figure 1 and Supplementary Figure 1, the 2 medial regions are combined. Tumors were counted visually and tumors greater than or less than 1 mm were scored by comparing size with a 1-mm diameter glass capillary tube. Tissue was frozen in Tissue-Tek OCT (Optimal Cutting Temperature) Compound (#62550-12; Electron Microscopy Sciences). Tissue used for RNA-Scope (ACD, Newark, CA) analysis was fixed in 4% PFA + PBS for 24 hours at 4ºC. Tissue used for gene expression analysis was placed in RNAlater buffer (Qiagen, Germantown, MD) at 4ºC overnight (O/N), then stored at -80ºC. Blood samples were collected in heparinized tubes, centrifuged to remove blood cells at room temperature, and then stored at -80ºC until analysis. Tnf and interleukin-6 blood cytokine measurements were performed by Eve Technologies (Calgary, Alberta, Canada). Corticosterone levels were determined by enzyme-linked immunosorbent assay (ADI-900-097; Enzo Life Sciences, Farmingdale, NY) in duplicate according to kit instructions at a 1:80 dilution with 1% steroid displacement buffer. Samples were assayed in 2 groups, with intra-assay variation of 7.3% and 7.7%, and interassay variation of a pooled mouse control was 9.5% and 9.3%.

Staining and Western Blot

Tissue was washed 3× in PBS and placed in 30% sucrose in PBS O/N. Tissue then was equilibrated in OCT for 1 hour and frozen at -80ºC. Tissue was sectioned at 10 μm using a Leica CM 1950 Cryostat (Leica Biosystems, Concord, Ontario). H&E staining and Alcian Blue staining was performed as per previous protocol.[46] Immunohistochemistry was performed as previously described.[46] Tumor dysplasia was blindly evaluated using a previously published scoring system: the number of adenomas and crypt architecture was assessed in the distal, medial, and proximal sites in the tissue, and the alteration in mucosa architecture, epithelial changes, hyperplasia, crypt abscesses, and crypt loss were scored from 0 to 4 (most severe) score.[98,99] 3,3′-Diaminobenzidine tetra hydrochloride staining was performed using horseradish peroxidase/3,3′-diaminobenzidine tetra hydrochloride (ABC) Detection IHC Kit as per the manufacturer's protocol (ab64261; Abcam). RNA in situ probe hybridization and detection was performed using the RNAScope method according to the manufacturer's protocol (ACD, Newark, CA). Antibodies used are shown in Table 1.

Tumors were microdissected, cut into small pieces, and then lysed in RIPA buffer containing Pierce Protease and Phosphatase Inhibitor (Pierce, Waltham, MA). Electrophoresis was performed on Mini-PROTEAN TGX Stain-free gels (Bio-Rad, Hercules, CA) and Western blot on polyvinylidene difluoride (Thermo Scientific, Waltham, MA). Western blot

Table 2. List of Quantitative Polymerase Chain Reaction Primers Used

Axin2	TGACTCTCCTTCCAGATCCCA	TGCCCACACTAGGCTGACA
Bmal1	TGACCCTCATGGAAGGTTAGAA	GGACATTGCATTGCATGTTGG
Ccnd1	GCGTACCCTGACACCAATCTC	CTCCTCTTCGCACTTCTGCTC
cMyc	ATGCCCCTCAACGTGAACTTC	GTCGCAGATGAAATAGGGCTG
Cry1	CACTGGTTCCGAAAGGGACTC	CTGAAGCAAAAATCGCCACCT
Dolk1	CAGTGTGGGACCGATACTCCT	CCAAGCAAAGGCATGACCA
Ereg	CTGCCTCTTGGGTCTTGACG	GCGGTACAGTTATCCTCGGATTC
Fam76b	GAATGTCGGATTGCACATCCT	GGTCTGAGGTGCTCCATATTTC
Gapdh	AGGTCGGTGTGAACGGATTTG	TGTAGACCATGTAGTTGAGGTCA
Golga1	AAGAATTGGATGCACGAACCA	AGCCGCTCGTTTAAGTCAGAT
Lgr5	CCTACTCGAAGACTTACCCAGT	GCATTGGGGTGAATGATAGCA
Msmo1	AAACAAAAGTGTTGGCGTGTTC	AAGCATTCTTAAAGGGCTCCTG
Mlixpl	AGATGGAGAACCGACGTATCA	ACTGAGCGTGCTGACAAGTC
Pmpca	CTGCACACAGACGGTTCAG	GTCCAGAGTGGTAACTTTGGTTT
Nr1d1	TGAACGCAGGAGGTGTGATTG	GAGGACTGGAAGCTATTCTCAGA
Rnf128	ATTCAAAGAGGCATCCAAGTCAC	TGCATTTCGTAATCTTCGAGCAG

were blocked for 30 minutes with 5% milk in PBS- and 0.1% Tween 20. Primary antibodies were incubated overnight at 4ºC. Secondary antibodies were incubated for 1 hour at room temperature. Horseradish peroxidase was developed using Super Signal Femto (Thermo Scientific) and imaged on a Bio-Rad gel Imager. All samples were collected at Zeitgeber Time 8. The antibodies used are shown in Table 1.

Microscopy

Samples were imaged using a slide scanner (Axio Scan.Z1; Zeiss, Toronto, Canada). The tumor area was quantified using Zen Blue Software (Zeiss). Organoid cloning images were obtained with a 5× objective on an AXIO Vert.A1 microscope (Zeiss). Images were processed using Adobe (San Jose, CA) Photoshop CS5. Antibody-positive cells were quantified as the total number of labeled cells or nuclei/total number of 4′,6-diamidino-2-phenylindole–positive nuclei. Ten crypts were sampled per animal for each intestinal region (proximal, medial, and distal) for quantification of PHH3, lysozyme, cleaved caspase-3, Ki67, Nr1d1, Yap, *Tead4*, *Lgr5*, *Ereg*, and *Axin2*. Regions were averaged together for results shown if no significant differences were observed.

RNA Purification

Tissue samples were homogenized using a bullet blender (Next Advance, Troy, NY), and RNA was isolated using the RNEasy mini Purification Kit (Qiagen). Complementary DNA was produced using the iScript RT Supermix (Bio-Rad) according to the manufacturer's protocol.

Quantitative Polymerase Chain Reaction

Transcript levels were quantified using iTaq Universal SYBR Green Supermix (Bio-Rad) on a Viia7 real-time polymerase chain reaction machine (Thermo Fisher Scientific). Primer sequences were obtained from PrimerBank (https://pga.mgh.harvard.edu/primerbank/) and validated at $r^2 \sim 0.98$, with an efficiency of approximately 80–110. The primers used are listed in Table 2.

Organoid Experiments

Intestinal organoids were derived from mice as previously reported.[46] For the 24-hour RNA sequencing, organoid biological replicates were collected every 2 hours (n = 2 derived lines of each of the 4 genotypes). For the 48-hour analyses, organoid biological replicates (n = 3 derived lines of each of the 4 genotypes) were collected every 4 hours. RNA sequencing experiments were performed by splitting organoids, allowing a 12-hour recovery, and then 1-hour treatment with 0.1 μm dexamethasone (Sigma, Oakville, Ontario) in base media containing epidermal growth factor. Media then was replaced with fresh organoid culture media. Samples were collected from 24 hours after dexamethasone treatment, every 2 hours, and immediately lysed in RLT (Qiagen) + 1% β-mecaptoethanol (M6250; Sigma Aldrich) and flash frozen in liquid nitrogen. For organoid cloning assays, 5 large organoids were selected from 1 animal of each genotype and dissociated for 10 minutes using 100 μL TrypLE Express (12605010; Thermo Fisher) + 1:1000 Y-27632 (72304; Stem Cell Tech, Vancouver, British Columbia). Enzymatic dissociation was quenched with 100-μL base organoid media containing epidermal growth factor + 1:1000 Y-27632. Single cells then were plated in ENR (EGF, Noggin, R-Spondin) / EN (EGF, Noggin) media + Y-27632 for 1 day. The following day, Y-27632 was removed and replaced with fresh ENR/EN media. Fast-growing Apc^{min} tumor organoids were quantified 5 days later, whereas slower-growing nontransformed organoids were quantified 15 days later. In all experiments, organoid media was changed every 2–5 days, depending on need. Yap chemical inhibition was performed using 3 mmol/

Table 3. Details of Statistical Tests

Panel	Test	Value	Panel	Test	Value
Figure 1					
A	Two-way ANOVA	$f_{(6, 52)} = 2.766$; $P = .0208$	J	Unpaired *t* test	$P < .0001$
C	One-way ANOVA Tukey post-test	$f_{(3, 46)} = 80.56$; $P < .0001$ $P < .0001$	K	Unpaired *t* test	$P = .7113$
D	One-way ANOVA Tukey post-test	$f_{(3, 47)} = 57.41$; $P < .0001$; $P < .0001$	L	Unpaired *t* test	$P = .5447$
F	Unpaired *t* test	$P = .0338$	M	Unpaired *t* test	$P = .4881$
H	One-way ANOVA Tukey post-test	$f_{(2, 390)} = 5.936$; $P = .0029$; ZT12 $P = .0030$	O	Unpaired *t* test	$P = .3793$
I	Unpaired *t* test	$P = .1036$			
Figure 2					
B	Unpaired *t* test	$P = .0012$	J	Unpaired *t* test	$P = .0013$
D	Unpaired *t* test	$P = .0166$	K	Unpaired *t* test	$P < .0001$
F	Two-way ANOVA Tukey post-test	$f_{(2, 218)} = 3.386$; $P = .0352$ ZT4 $P = .0246$	L	Unpaired *t* test	$P = .0123$
G	Unpaired *t* test	$P = .031$	N	Unpaired *t* test	$P = .0005$
I	Unpaired *t* test	$P = .1409$	P	Unpaired *t* test	$P < .0001$
Figure 3					
C	MetaCycle2d	Nr1d1 ($P = 4.9^{-08}$; $q = 0.00039$), Cry1 ($P = 3.8^{-08}$; $q = 0.00039$), Bmp3 ($P = .00012$; $q = 0.057$), Ephb3 ($P = 8.0^{-06}$; $q = 0.0084$), Kit ($P = .00016$; $q = 0.067$), Tead4 ($P = 1.09^{-05}$; $q = 0.0098$)			
D	Two-way ANOVA	Nr1d1 ($f_{(12, 37)} = 5.993$; $P < .0001$), Cry1 ($f_{(1, 37)} = 413.1$; $P < .0001$), Tead4 ($f_{(12, 37)} = 15.36$; $P < .0001$)			
Figure 4					
D	MetaCycle2d	Golga ($P = 1.20^{-06}$; $q = 0.015$), Dolk ($P = 2.83^{-06}$; $q = 0.015$), RNF128 ($P = 5.81^{-06}$; $q = 0.015$), Mlxipl ($P = 4.26^{-07}$; $q = 0.0053$), Msmo1 ($P = 1.04^{-06}$; $q = 0.0053$), Fam76b ($P = 1.44^{-06}$; $q = 0.0055$)			
E	Two-way ANOVA	Golga ($f_{(12, 26)} = 8.393$; $P < .0001$), Dolk ($f_{(12, 26)} = 3.557$; $P = .0033$) RNF128 ($f_{12, 25)} = 3.284$; $P = .0058$), Mlxipl ($f_{(12,15)} = 1.220$; $P = .3623$), Msmo1($f_{12, 13)} = 2.051$; $P = .1067$), Fam76b ($f_{(12, 26)} = 6.062$; $P < .0001$)			
Figure 5					
A	Gene-wise 1-way ANOVA (4 genotypes) with BH correction Gene-wise Tukey post-test (2 genotypes) with BH correction	$f_{(3,84)} > 2.75$; $P < .047$; $q < 0.05$; $P < .00357$; $q < 0.05$	H	Unpaired *t* test	$P = .0075$
B	Gene-wise 1-way ANOVA (4 genotypes) with BH correction Gene-wise Tukey post-test (2 genotypes) with BH correction	$f_{(3,84)} > 2.75$; $P < .047$; $q < 0.05$; $P < .02815$; $q < 0.05$	K	Unpaired *t* test	$P = .0444$
C	GO analysis: DAVID 6.8	$P < .0002$; Benjamini < 0.05 Gene set > 9	L	One-way ANOVA Tukey post-test *Apc*^{min}; *Bmal1*$^{-/-}$DMSO vs Yap-i	$f_{(3, 10)} = 19.55$; $P = .0002$; $P = .0068$
D	ES NES Nominal *P* value FDR *q*-value FWER *P* value	ES, 0.44; NES, 2.083; $P = .000$; $q = 0.000$; $P = .000$	M.	One-way ANOVA Tukey post-test: DMSO vs DMSO *Apc*^{min}; *Bmal1*$^{-/-}$DMSO vs YAP	$f_{(2,43)} = 4.69$; $P = .0144$; $P = .0272$; $P = .0044$
G	Unpaired *t* test	$P = .0004$			
Figure 6					
A	One-way ANOVA Tukey post-test	$f_{(3,8)} = 11.48$; $P = .0026$; $P = .0029$	D	One-way ANOVA Tukey post-test	$f_{(3, 16)} = 8.420$; $P = .0014$; $P = .0217$
B	Unpaired *t* test	0.9172	F	One-way ANOVA Tukey post-test	$f_{(3, 65)} = 6.824$; $P = .005$; $P = .0182$
C	Unpaired *t* test	$P = .027$			

Table 3. Continued

Panel	Test	Value	Panel	Test	Value
Figure 7					
B	Unpaired *t* test	$P = .0186$	G	One-way ANOVA Sidak post-test	$f_{(3, 36)} = 9.241$; $P = .0001$ $P = .0096$
E	Unpaired *t* test	$P = .0009$	I	One-way ANOVA Sidak post-test	$f_{(3, 36)} = 9.422$; $P < .0001$ $P = .0064$
D	Unpaired *t* test	$P = .027$			
Figure 8					
A	Two-way ANOVA	$f_{(5, 168)} = 12.01$; $P < .0001$	H	Two-way ANOVA Tukey post-test	$f_{(2, 116)} = 351.9$; $P < .0001$ ZT4 $P < .0001$ ZT12 $P < .0001$
C	Two-way ANOVA	$f_{(5, 168)} = 6.49$; $P < .0001$	J	Mixed-effect analysis Sidak post-test	$f_{(2, 27)} = 127.4$; $P < .0001$ ZT12 < 0.0001
E	Two-way ANOVA	$f_{(1, 168)} = 25.50$; $P < .0001$			

Panel	Test	Value
Figure 9		
A	Two-way ANOVA	$f_{(5, 168)} = 2.50$; $P = .033$
C	Two-way ANOVA	$f_{(5, 168)} = 9.24$; $P = .0027$
E	Two-way ANOVA	$f_{(1, 168)} = 8.947$; $P = .0032$
G	Two-way ANOVA	$f_{(1, 168)} = 71.98$; $P < .0001$
I	Two-way ANOVA	$f_{(1, 168)} = 41.51$; $P < .0001$
K	Two-way ANOVA	$F_{(5, 168)} = 2.746$; $P = .02$

Panel	Test	Value	Panel	Test	Value
Figure 10					
B	One-way ANOVA Tukey post-test	$f_{(3, 20)} = 20.58$; $P < .0001$ $P = .0027$	G	Unpaired *t* test	$P = .0341$
C	One-way ANOVA Tukey post-test	$f_{(3, 20)} = 28.71$; $P < .0001$ $P = .0014$	I	Unpaired *t* test	$P = .0447$
E	Unpaired *t* test	$P = .0023$			

ANOVA, analysis of variance; DMSO, dimethyl sulfoxide; ES, enrichment score; FDR, False Discovery Rate; FWER, Family-Wise Error Rate; NES, normalized enrichment score; Yap-i, Yap Inhibitor; ZT, Zeitgeber Time.

L Verteporfin (AOB5623; Aobious, Gloucester, MA), Tead inhibition using 3 mmol/L TED-347 (AOB17707; Aobious), and 1:750 dimethyl sulfoxide vehicle control (D2650; Sigma) was applied to organoid media.

RNA Sequencing and Gene Expression Analysis

A total of 1 μg RNA per sample was prepared at the Donnelly Sequencing Centre (http://ccbr.utoronto.ca/donnelly-sequencing-centre) for RNA integrity assessment and sequencing. Libraries were prepared using 96 NEB–NEBNext Ultra II Directional RNA Library Prep Kit including quality control and DNase treatment (#E7765; New England Biolabs, Ipswich, MA). Sequencing was performed on a 1 Flowcell, Illumina NovaSeq6000 (Illumina), S2; 100 cycles; v1 chemistry read 1, 101 bp; index read 1, 8 bp; and index read 2, 8 bp. Raw transcriptome sequencing reads were aligned against GRCm38 and Ensembl release 96 transcript annotations using STAR v2.5.[100] RSEM v1.3.0[101] was used for transcript quantification. Libraries were excluded from further analyses in the case of low-quality alignment (Supplementary Table 4). Transcripts per million values for all remaining libraries in each genotype were merged into 1 expression table file. Quantile normalization was performed for each expression table using the preprocessCore package. Rhythmic analysis and differential expression analysis were performed as follows. First, genes with null expression in at least 1 sample within a table were excluded from that table. Rhythmicity for the remaining transcripts then was evaluated with MetaCycle,[57] and we considered all transcripts with a base expression greater than 0.5, relative amplitude greater than 0.05, and a BH q value less than 0.1 as rhythmic. The number of rhythmic transcripts was as follows: 41 in control organoids, 0 in *Bmal1* mutant, 238 in Apc^{min} control, and 263 in Apc^{min} + *Bmal1* mutant (Supplementary Table 1). We next evaluated gene-by-gene (n = 17,543) the differences in overall expression across 24 hours (all time points) between genotypes/expression tables, using analysis of variance (ANOVA), followed by the post hoc Tukey test. For each gene, pairwise expression fold changes between genotypes were calculated as the ratio between the average 24-hour expression in the first genotype and the average in the second genotype. With a Tukey q value less than 0.05 and |log2(fold change)| greater than 1.5, the number of differentially expressed genes was as follows: 111 between control and *Bmal1* mutant, 6405 between control and Apc^{min} control, and 2398 between Apc^{min}

control and Apc^{min} + *Bmal1* mutant (Supplementary Table 2). GSEA was conducted in the GSEA 4.1.0 software downloaded from https://www.gsea-msigdb.org/gsea/index.jsp. Genes selected to be input into GSEA had to be expressed in two thirds of the samples (Supplementary Table 5). The gene set (size = 425) for GSEA analysis was generated using genes found to be up-regulated 2-fold or greater in[43] RNA sequencing data set.

Statistics

Statistical analysis was performed using Prism 8 (GraphPad, San Diego, CA). An unpaired *t* test, 1-way ANOVA, or 2-way ANOVA were used with a post-test (Table 3). RNA sequencing data analyses were performed in R. MetaCycle was applied using JTK and LS algorithms and the Fisher method for *P* value integration. For comparisons between genotypes, the *P* values from ANOVA and the post hoc Tukey tests were corrected with the BH method. In these tests, genes that were absent in any 1 genotype were assigned the lowest expression value found in the expression tables. Pearson heatmaps were plotted using the Python 3.6–Seaborn library based on the Pearson correlation between the participant genes. Cubic spline interpolation was used to model the growth of a gene throughout time points (Figures 8 and 9). The splines are natural where the first derivative $\partial 1$ and the second derivative $\partial 2$ both equal 0 at each time point. Implementation of the cubic spline interpolation was performed using Matlab 2013a.

References

1. Hanahan D, Weinberg RA. Hallmarks of cancer: the next generation. Cell 2011;144:646–674.
2. Takahashi JS. Transcriptional architecture of the mammalian circadian clock. Nat Rev Genet 2017; 18:164–179.
3. Zhang R, Lahens NF, Ballance HI, Hughes ME, Hogenesch JB. A circadian gene expression atlas in mammals: implications for biology and medicine. Proc Natl Acad Sci U S A 2014;111:16219–16224.
4. Bass J, Lazar MA. Circadian time signatures of fitness and disease. Science 2016;354:994–999.
5. Janich P, Meng QJ, Benitah SA. Circadian control of tissue homeostasis and adult stem cells. Curr Opin Cell Biol 2014;31C:8–15.
6. Schernhammer ES, Laden F, Speizer FE, Willett WC, Hunter DJ, Kawachi I, Colditz GA. Rotating night shifts and risk of breast cancer in women participating in the nurses' health study. J Natl Cancer Inst 2001; 93:1563–1568.
7. Schernhammer ES, Laden F, Speizer FE, Willett WC, Hunter DJ, Kawachi I, Fuchs CS, Colditz GA. Night-shift work and risk of colorectal cancer in the nurses' health study. J Natl Cancer Inst 2003;95:825–828.
8. Flynn-Evans EE, Mucci L, Stevens RG, Lockley SW. Shiftwork and prostate-specific antigen in the National Health and Nutrition Examination Survey. J Natl Cancer Inst 2013;105:1292–1297.
9. Wegrzyn LR, Tamimi RM, Rosner BA, Brown SB, Stevens RG, Eliassen AH, Laden F, Willett WC, Hankinson SE, Schernhammer ES. Rotating night-shift work and the risk of breast cancer in the Nurses' Health Studies. Am J Epidemiol 2017;186:532–540.
10. Um K, Park CS, Yoo C, Ahn YS, Kim M, Jeong KS. Risk factors including night shift work of colorectal polyp. Ann Occup Environ Med 2020;32:e26.
11. Sancar A, Lindsey-Boltz LA, Gaddameedhi S, Selby CP, Ye R, Chiou YY, Kemp MG, Hu J, Lee JH, Ozturk N. Circadian clock, cancer, and chemotherapy. Biochemistry 2015;54:110–123.
12. Masri S, Sassone-Corsi P. The emerging link between cancer, metabolism, and circadian rhythms. Nat Med 2018;24:1795–1803.
13. Yu EA, Weaver DR. Disrupting the circadian clock: gene-specific effects on aging, cancer, and other phenotypes. Aging (Albany NY) 2011;3:479–493.
14. Sancar A, Van Gelder RN. Clocks, cancer, and chronochemotherapy. Science 2021;371:eabb0738.
15. Alhopuro P, Bjorklund M, Sammalkorpi H, Turunen M, Tuupanen S, Bistrom M, Niittymaki I, Lehtonen HJ, Kivioja T, Launonen V, Saharinen J, Nousiainen K, Hautaniemi S, Nuorva K, Mecklin JP, Jarvinen H, Orntoft T, Arango D, Lehtonen R, Karhu A, Taipale J, Aaltonen LA. Mutations in the circadian gene CLOCK in colorectal cancer. Mol Cancer Res 2010;8:952–960.
16. Momma T, Okayama H, Saitou M, Sugeno H, Yoshimoto N, Takebayashi Y, Ohki S, Takenoshita S. Expression of circadian clock genes in human colorectal adenoma and carcinoma. Oncol Lett 2017; 14:5319–5325.
17. Wang X, Yan D, Teng M, Fan J, Zhou C, Li D, Qiu G, Sun X, Li T, Xing T, Tang H, Peng X, Peng Z. Reduced expression of PER3 is associated with incidence and development of colon cancer. Ann Surg Oncol 2012; 19:3081–3088.
18. Lellupitiyage Don SS, Lin HH, Furtado JJ, Qraitem M, Taylor SR, Farkas ME. Circadian oscillations persist in low malignancy breast cancer cells. Cell Cycle 2019; 18:2447–2453.
19. Broadberry E, McConnell J, Williams J, Yang N, Zindy E, Leek A, Waddington R, Joseph L, Howe M, Meng QJ, Streuli CH. Disrupted circadian clocks and altered tissue mechanics in primary human breast tumours. Breast Cancer Res 2018;20:125.
20. Altman BJ, Hsieh AL, Sengupta A, Krishnanaiah SY, Stine ZE, Walton ZE, Gouw AM, Venkataraman A, Li B, Goraksha-Hicks P, Diskin SJ, Bellovin DI, Simon MC, Rathmell JC, Lazar MA, Maris JM, Felsher DW, Hogenesch JB, Weljie AM, Dang CV. MYC disrupts the circadian clock and metabolism in cancer cells. Cell Metab 2015;22:1009–1019.
21. Marcheva B, Ramsey KM, Buhr ED, Kobayashi Y, Su H, Ko CH, Ivanova G, Omura C, Mo S, Vitaterna MH, Lopez JP, Philipson LH, Bradfield CA, Crosby SD, JeBailey L, Wang X, Takahashi JS, Bass J. Disruption of the clock components CLOCK and BMAL1 leads to hypoinsulinaemia and diabetes. Nature 2010; 466:627–631.

22. Kowalska E, Ripperger JA, Hoegger DC, Bruegger P, Buch T, Birchler T, Mueller A, Albrecht U, Contaldo C, Brown SA. NONO couples the circadian clock to the cell cycle. Proc Natl Acad Sci U S A 2013;110:1592–1599.
23. Plikus MV, Vollmers C, de la Cruz D, Chaix A, Ramos R, Panda S, Chuong CM. Local circadian clock gates cell cycle progression of transient amplifying cells during regenerative hair cycling. Proc Natl Acad Sci U S A 2013; 110:E2106–E2115.
24. Lee JH, Sancar A. Circadian clock disruption improves the efficacy of chemotherapy through p73-mediated apoptosis. Proc Natl Acad Sci U S A 2011; 108:10668–10672.
25. Lee JH, Sancar A. Regulation of apoptosis by the circadian clock through NF-kappaB signaling. Proc Natl Acad Sci U S A 2011;108:12036–12041.
26. Gaddameedhi S, Selby CP, Kaufmann WK, Smart RC, Sancar A. Control of skin cancer by the circadian rhythm. Proc Natl Acad Sci U S A 2011;108:18790–18795.
27. Gery S, Komatsu N, Baldjyan L, Yu A, Koo D, Koeffler HP. The circadian gene per1 plays an important role in cell growth and DNA damage control in human cancer cells. Mol Cell 2006;22:375–382.
28. Fu L, Pelicano H, Liu J, Huang P, Lee C. The circadian gene Period2 plays an important role in tumor suppression and DNA damage response in vivo. Cell 2002; 111:41–50.
29. Wood PA, Yang X, Taber A, Oh EY, Ansell C, Ayers SE, Al-Assaad Z, Carnevale K, Berger FG, Pena MM, Hrushesky WJ. Period 2 mutation accelerates ApcMin/+ tumorigenesis. Mol Cancer Res 2008;6:1786–1793.
30. Papagiannakopoulos T, Bauer MR, Davidson SM, Heimann M, Subbaraj L, Bhutkar A, Bartlebaugh J, Vander Heiden MG, Jacks T. Circadian rhythm disruption promotes lung tumorigenesis. Cell Metab 2016; 24:324–331.
31. Mteyrek A, Filipski E, Guettier C, Okyar A, Levi F. Clock gene Per2 as a controller of liver carcinogenesis. Oncotarget 2016;7:85832–85847.
32. Antoch MP, Toshkov I, Kuropatwinski KK, Jackson M. Deficiency in PER proteins has no effect on the rate of spontaneous and radiation-induced carcinogenesis. Cell Cycle 2013;12:3673–3680.
33. Roenneberg T, Merrow M. The circadian clock and human health. Curr Biol 2016;26:R432–R443.
34. Moser AR, Pitot HC, Dove WF. A dominant mutation that predisposes to multiple intestinal neoplasia in the mouse. Science 1990;247:322–324.
35. Su LK, Kinzler KW, Vogelstein B, Preisinger AC, Moser AR, Luongo C, Gould KA, Dove WF. Multiple intestinal neoplasia caused by a mutation in the murine homolog of the APC gene. Science 1992;256:668–670.
36. Medema JP, Vermeulen L. Microenvironmental regulation of stem cells in intestinal homeostasis and cancer. Nature 2011;474:318–326.
37. Barker N, Ridgway RA, van Es JH, van de Wetering M, Begthel H, van den Born M, Danenberg E, Clarke AR, Sansom OJ, Clevers H. Crypt stem cells as the cells-of-origin of intestinal cancer. Nature 2009;457:608–611.
38. Gehart H, Clevers H. Tales from the crypt: new insights into intestinal stem cells. Nat Rev Gastroenterol Hepatol 2019;16:19–34.
39. Karin M, Clevers H. Reparative inflammation takes charge of tissue regeneration. Nature 2016; 529:307–315.
40. Grivennikov SI, Greten FR, Karin M. Immunity, inflammation, and cancer. Cell 2010;140:883–899.
41. Wang Y, Chiang IL, Ohara TE, Fujii S, Cheng J, Muegge BD, Ver Heul A, Han ND, Lu Q, Xiong S, Chen F, Lai CW, Janova H, Wu R, Whitehurst CE, VanDussen KL, Liu TC, Gordon JI, Sibley LD, Stappenbeck TS. Long-term culture captures injury-repair cycles of colonic stem cells. Cell 2019;179:1144–1159 e15.
42. Yui S, Azzolin L, Maimets M, Pedersen MT, Fordham RP, Hansen SL, Larsen HL, Guiu J, Alves MRP, Rundsten CF, Johansen JV, Li Y, Madsen CD, Nakamura T, Watanabe M, Nielsen OH, Schweiger PJ, Piccolo S, Jensen KB. YAP/TAZ-dependent reprogramming of colonic epithelium links ECM remodeling to tissue regeneration. Cell Stem Cell 2018;22:35–49 e7.
43. Gregorieff A, Liu Y, Inanlou MR, Khomchuk Y, Wrana JL. Yap-dependent reprogramming of Lgr5(+) stem cells drives intestinal regeneration and cancer. Nature 2015; 526:715–718.
44. Taniguchi K, Wu LW, Grivennikov SI, de Jong PR, Lian I, Yu FX, Wang K, Ho SB, Boland BS, Chang JT, Sandborn WJ, Hardiman G, Raz E, Maehara Y, Yoshimura A, Zucman-Rossi J, Guan KL, Karin M. A gp130-Src-YAP module links inflammation to epithelial regeneration. Nature 2015;519:57–62.
45. Romera-Hernandez M, Aparicio-Domingo P, Papazian N, Karrich JJ, Cornelissen F, Hoogenboezem RM, Samsom JN, Cupedo T. Yap1-driven intestinal repair is controlled by group 3 innate lymphoid cells. Cell Rep 2020;30:37–45 e3.
46. Stokes K, Cooke A, Chang H, Weaver DR, Breault DT, Karpowicz P. The circadian clock gene BMAL1 coordinates intestinal regeneration. Cell Mol Gastroenterol Hepatol 2017;4:95–114.
47. Parasram K, Bernardon N, Hammoud M, Chang H, He L, Perrimon N, Karpowicz P. Intestinal stem cells exhibit conditional circadian clock function. Stem Cell Rep 2018;11:1287–1301.
48. Karpowicz P, Zhang Y, Hogenesch JB, Emery P, Perrimon N. The circadian clock gates the intestinal stem cell regenerative state. Cell Rep 2013;3:996–1004.
49. Janich P, Pascual G, Merlos-Suarez A, Batlle E, Ripperger J, Albrecht U, Cheng HY, Obrietan K, Di Croce L, Benitah SA. The circadian molecular clock creates epidermal stem cell heterogeneity. Nature 2011; 480:209–214.
50. Bunger MK, Wilsbacher LD, Moran SM, Clendenin C, Radcliffe LA, Hogenesch JB, Simon MC, Takahashi JS, Bradfield CA. Mop3 is an essential component of the master circadian pacemaker in mammals. Cell 2000; 103:1009–1017.
51. Kondratov RV, Kondratova AA, Gorbacheva VY, Vykhovanets OV, Antoch MP. Early aging and age-related pathologies in mice deficient in BMAL1, the

core component of the circadian clock. Genes Dev 2006; 20:1868–1873.

52. Balsalobre A, Brown SA, Marcacci L, Tronche F, Kellendonk C, Reichardt HM, Schutz G, Schibler U. Resetting of circadian time in peripheral tissues by glucocorticoid signaling. Science 2000;289:2344–2347.
53. Leliavski A, Shostak A, Husse J, Oster H. Impaired glucocorticoid production and response to stress in Arntl-deficient male mice. Endocrinology 2014; 155:133–142.
54. Matsu-Ura T, Dovzhenok A, Aihara E, Rood J, Le H, Ren Y, Rosselot AE, Zhang T, Lee C, Obrietan K, Montrose MH, Lim S, Moore SR, Hong CI. Intercellular coupling of the cell cycle and circadian clock in adult stem cell culture. Mol Cell 2016;64:900–912.
55. Imajo M, Ebisuya M, Nishida E. Dual role of YAP and TAZ in renewal of the intestinal epithelium. Nat Cell Biol 2015; 17:7–19.
56. Hughes ME, Abruzzi KC, Allada R, Anafi R, Arpat AB, Asher G, Baldi P, de Bekker C, Bell-Pedersen D, Blau J, Brown S, Ceriani MF, Chen Z, Chiu JC, Cox J, Crowell AM, DeBruyne JP, Dijk DJ, DiTacchio L, Doyle FJ, Duffield GE, Dunlap JC, Eckel-Mahan K, Esser KA, FitzGerald GA, Forger DB, Francey LJ, Fu YH, Gachon F, Gatfield D, de Goede P, Golden SS, Green C, Harer J, Harmer S, Haspel J, Hastings MH, Herzel H, Herzog ED, Hoffmann C, Hong C, Hughey JJ, Hurley JM, de la Iglesia HO, Johnson C, Kay SA, Koike N, Kornacker K, Kramer A, Lamia K, Leise T, Lewis SA, Li J, Li X, Liu AC, Loros JJ, Martino TA, Menet JS, Merrow M, Millar AJ, Mockler T, Naef F, Nagoshi E, Nitabach MN, Olmedo M, Nusinow DA, Ptáček LJ, Rand D, Reddy AB, Robles MS, Roenneberg T, Rosbash M, Ruben MD, Rund SSC, Sancar A, Sassone-Corsi P, Sehgal A, Sherrill-Mix S, Skene DJ, Storch KF, Takahashi JS, Ueda HR, Wang H, Weitz C, Westermark PO, Wijnen H, Xu Y, Wu G, Yoo SH, Young M, Zhang EE, Zielinski T, Hogenesch JB. Guidelines for genome-scale analysis of biological rhythms. J Biol Rhythms 2017; 32:380–393.
57. Wu G, Anafi RC, Hughes ME, Kornacker K, Hogenesch JB. MetaCycle: an integrated R package to evaluate periodicity in large scale data. Bioinformatics 2016;32:3351–3353.
58. De Vos M, Schreiber V, Dantzer F. The diverse roles and clinical relevance of PARPs in DNA damage repair: current state of the art. Biochem Pharmacol 2012; 84:137–146.
59. Schmitt M, Schewe M, Sacchetti A, Feijtel D, van de Geer WS, Teeuwssen M, Sleddens HF, Joosten R, van Royen ME, van de Werken HJG, van Es J, Clevers H, Fodde R. Paneth cells respond to inflammation and contribute to tissue regeneration by acquiring stem-like features through SCF/c-Kit signaling. Cell Rep 2018; 24:2312–2328 e7.
60. Moor AE, Harnik Y, Ben-Moshe S, Massasa EE, Rozenberg M, Eilam R, Bahar Halpern K, Itzkovitz S. Spatial reconstruction of single enterocytes uncovers broad zonation along the intestinal villus axis. Cell 2018; 175:1156–1167 e15.
61. Subramanian A, Tamayo P, Mootha VK, Mukherjee S, Ebert BL, Gillette MA, Paulovich A, Pomeroy SL, Golub TR, Lander ES, Mesirov JP. Gene set enrichment analysis: a knowledge-based approach for interpreting genome-wide expression profiles. Proc Natl Acad Sci U S A 2005;102:15545–15550.
62. Kreso A, Dick JE. Evolution of the cancer stem cell model. Cell Stem Cell 2014;14:275–291.
63. Schwitalla S, Fingerle AA, Cammareri P, Nebelsiek T, Goktuna SI, Ziegler PK, Canli O, Heijmans J, Huels DJ, Moreaux G, Rupec RA, Gerhard M, Schmid R, Barker N, Clevers H, Lang R, Neumann J, Kirchner T, Taketo MM, van den Brink GR, Sansom OJ, Arkan MC, Greten FR. Intestinal tumorigenesis initiated by dedifferentiation and acquisition of stem-cell-like properties. Cell 2013; 152:25–38.
64. Sato T, Vries RG, Snippert HJ, van de Wetering M, Barker N, Stange DE, van Es JH, Abo A, Kujala P, Peters PJ, Clevers H. Single Lgr5 stem cells build crypt-villus structures in vitro without a mesenchymal niche. Nature 2009;459:262–265.
65. Serra D, Mayr U, Boni A, Lukonin I, Rempfler M, Challet Meylan L, Stadler MB, Strnad P, Papasaikas P, Vischi D, Waldt A, Roma G, Liberali P. Self-organization and symmetry breaking in intestinal organoid development. Nature 2019;569:66–72.
66. Bum-Erdene K, Zhou D, Gonzalez-Gutierrez G, Ghozayel MK, Si Y, Xu D, Shannon HE, Bailey BJ, Corson TW, Pollok KE, Wells CD, Meroueh SO. Small-molecule covalent modification of conserved cysteine leads to allosteric inhibition of the TEAD·Yap protein-protein interaction. Cell Chem Biol 2019;26:378–389. e13.
67. Madison BB, Dunbar L, Qiao XT, Braunstein K, Braunstein E, Gumucio DL. Cis elements of the villin gene control expression in restricted domains of the vertical (crypt) and horizontal (duodenum, cecum) axes of the intestine. J Biol Chem 2002;277:33275–33283.
68. Storch KF, Paz C, Signorovitch J, Raviola E, Pawlyk B, Li T, Weitz CJ. Intrinsic circadian clock of the mammalian retina: importance for retinal processing of visual information. Cell 2007;130:730–741.
69. Wang S, Lin Y, Yuan X, Li F, Guo L, Wu B. REV-ERBalpha integrates colon clock with experimental colitis through regulation of NF-kappaB/NLRP3 axis. Nat Commun 2018;9:4246.
70. Pagel R, Bar F, Schroder T, Sunderhauf A, Kunstner A, Ibrahim SM, Autenrieth SE, Kalies K, Konig P, Tsang AH, Bettenworth D, Divanovic S, Lehnert H, Fellermann K, Oster H, Derer S, Sina C. Circadian rhythm disruption impairs tissue homeostasis and exacerbates chronic inflammation in the intestine. FASEB J 2017; 31:4707–4719.
71. Panda S. Circadian physiology of metabolism. Science 2016;354:1008–1015.
72. Lucassen EA, Coomans CP, van Putten M, de Kreij SR, van Genugten JH, Sutorius RP, de Rooij KE, van der Velde M, Verhoeve SL, Smit JW, Lowik CW, Smits HH,

Guigas B, Aartsma-Rus AM, Meijer JH. Environmental 24-hr cycles are essential for health. Curr Biol 2016; 26:1843–1853.

73. Pendergast JS, Friday RC, Yamazaki S. Distinct functions of Period2 and Period3 in the mouse circadian system revealed by in vitro analysis. PLoS One 2010;5: e8552.
74. Hashikawa KI, Katamune C, Kusunose N, Matsunaga N, Koyanagi S, Ohdo S. Dysfunction of the circadian transcriptional factor CLOCK in mice resists chemical carcinogen-induced tumorigenesis. Sci Rep 2017; 7:9995.
75. Sulli G, Rommel A, Wang X, Kolar MJ, Puca F, Saghatelian A, Plikus MV, Verma IM, Panda S. Pharmacological activation of REV-ERBs is lethal in cancer and oncogene-induced senescence. Nature 2018; 553:351–355.
76. Puram RV, Kowalczyk MS, de Boer CG, Schneider RK, Miller PG, McConkey M, Tothova Z, Tejero H, Heckl D, Jaras M, Chen MC, Li H, Tamayo A, Cowley GS, Rozenblatt-Rosen O, Al-Shahrour F, Regev A, Ebert BL. Core circadian clock genes regulate leukemia stem cells in AML. Cell 2016;165:303–316.
77. Dong Z, Zhang G, Qu M, Gimple RC, Wu Q, Qiu Z, Prager BC, Wang X, Kim LJY, Morton AR, Dixit D, Zhou W, Huang H, Li B, Zhu Z, Bao S, Mack SC, Chavez L, Kay SA, Rich JN. Targeting glioblastoma stem cells through disruption of the circadian clock. Cancer Discov 2019;9:1556–1573.
78. Brown SA, Zumbrunn G, Fleury-Olela F, Preitner N, Schibler U. Rhythms of mammalian body temperature can sustain peripheral circadian clocks. Curr Biol 2002; 12:1574–1583.
79. Das M, Ellies LG, Kumar D, Sauceda C, Oberg A, Gross E, Mandt T, Newton IG, Kaur M, Sears DD, Webster NJG. Time-restricted feeding normalizes hyperinsulinemia to inhibit breast cancer in obese postmenopausal mouse models. Nat Commun 2021; 12:565.
80. Filipski E, Levi F. Circadian disruption in experimental cancer processes. Integr Cancer Ther 2009;8:298–302.
81. Chaix A, Lin T, Le HD, Chang MW, Panda S. Time-restricted feeding prevents obesity and metabolic syndrome in mice lacking a circadian clock. Cell Metab 2018;29:303–319.e4.
82. Repouskou A, Prombona A. c-MYC targets the central oscillator gene Per1 and is regulated by the circadian clock at the post-transcriptional level. Biochim Biophys Acta 2016;1859:541–552.
83. Shostak A, Ruppert B, Ha N, Bruns P, Toprak UH, Project IM-S, Eils R, Schlesner M, Diernfellner A, Brunner M. MYC/MIZ1-dependent gene repression inversely coordinates the circadian clock with cell cycle and proliferation. Nat Commun 2016;7:11807.
84. Ko CH, Yamada YR, Welsh DK, Buhr ED, Liu AC, Zhang EE, Ralph MR, Kay SA, Forger DB, Takahashi JS. Emergence of noise-induced oscillations in the central circadian pacemaker. PLoS Biol 2010;8:e1000513.
85. Ray S, Valekunja UK, Stangherlin A, Howell SA, Snijders AP, Damodaran G, Reddy AB. Circadian rhythms in the absence of the clock gene Bmal1. Science 2020;367:800–806.
86. Krishnaiah SY, Wu G, Altman BJ, Growe J, Rhoades SD, Coldren F, Venkataraman A, Olarerin-George AO, Francey LJ, Mukherjee S, Girish S, Selby CP, Cal S, Er U, Sianati B, Sengupta A, Anafi RC, Kavakli IH, Sancar A, Baur JA, Dang CV, Hogenesch JB, Weljie AM. Clock regulation of metabolites reveals coupling between transcription and metabolism. Cell Metab 2017; 25:961–974 e4.
87. Sladek M, Rybova M, Jindrakova Z, Zemanova Z, Polidarova L, Mrnka L, O'Neill J, Pacha J, Sumova A. Insight into the circadian clock within rat colonic epithelial cells. Gastroenterology 2007;133:1240–1249.
88. Hoogerwerf WA, Hellmich HL, Cornelissen G, Halberg F, Shahinian VB, Bostwick J, Savidge TC, Cassone VM. Clock gene expression in the murine gastrointestinal tract: endogenous rhythmicity and effects of a feeding regimen. Gastroenterology 2007;133:1250–1260.
89. Hoogerwerf WA, Sinha M, Conesa A, Luxon BA, Shahinian VB, Cornelissen G, Halberg F, Bostwick J, Timm J, Cassone VM. Transcriptional profiling of mRNA expression in the mouse distal colon. Gastroenterology 2008;135:2019–2029.
90. Thaiss CA, Levy M, Korem T, Dohnalova L, Shapiro H, Jaitin DA, David E, Winter DR, Gury-BenAri M, Tatirovsky E, Tuganbaev T, Federici S, Zmora N, Zeevi D, Dori-Bachash M, Pevsner-Fischer M, Kartvelishvily E, Brandis A, Harmelin A, Shibolet O, Halpern Z, Honda K, Amit I, Segal E, Elinav E. Microbiota diurnal rhythmicity programs host transcriptome oscillations. Cell 2016;167:1495–1510 e12.
91. Weger BD, Gobet C, Yeung J, Martin E, Jimenez S, Betrisey B, Foata F, Berger B, Balvay A, Foussier A, Charpagne A, Boizet-Bonhoure B, Chou CJ, Naef F, Gachon F. The mouse microbiome is required for sex-specific diurnal rhythms of gene expression and metabolism. Cell Metab 2019;29:362–382 e8.
92. Kuang Z, Wang Y, Li Y, Ye C, Ruhn KA, Behrendt CL, Olson EN, Hooper LV. The intestinal microbiota programs diurnal rhythms in host metabolism through histone deacetylase 3. Science 2019;365:1428–1434.
93. Liang X, Bushman FD, FitzGerald GA. Rhythmicity of the intestinal microbiota is regulated by gender and the host circadian clock. Proc Natl Acad Sci U S A 2015; 112:10479–10484.
94. Man K, Loudon A, Chawla A. Immunity around the clock. Science 2016;354:999–1003.
95. Kiessling S, Beaulieu-Laroche L, Blum ID, Landgraf D, Welsh DK, Storch KF, Labrecque N, Cermakian N. Enhancing circadian clock function in cancer cells inhibits tumor growth. BMC Biol 2017;15:13.
96. Bishehsari F, Voigt RM, Keshavarzian A. Circadian rhythms and the gut microbiota: from the metabolic syndrome to cancer. Nat Rev Endocrinol 2020;16:731–739.
97. Ayyaz A, Kumar S, Sangiorgi B, Ghoshal B, Gosio J, Ouladan S, Fink M, Barutcu S, Trcka D, Shen J, Chan K, Wrana JL, Gregorieff A. Single-cell transcriptomes of the regenerating intestine reveal a revival stem cell. Nature 2019;569:121–125.

98. Raufman JP, Shant J, Xie G, Cheng K, Gao XM, Shiu B, Shah N, Drachenberg CB, Heath J, Wess J, Khurana S. Muscarinic receptor subtype-3 gene ablation and scopolamine butylbromide treatment attenuate small intestinal neoplasia in Apcmin/+ mice. Carcinogenesis 2011;32:1396–1402.
99. Erben U, Loddenkemper C, Doerfel K, Spieckermann S, Haller D, Heimesaat MM, Zeitz M, Siegmund B, Kuhl AA. A guide to histomorphological evaluation of intestinal inflammation in mouse models. Int J Clin Exp Pathol 2014;7:4557–4576.
100. Dobin A, Davis CA, Schlesinger F, Drenkow J, Zaleski C, Jha S, Batut P, Chaisson M, Gingeras TR. STAR: ultrafast universal RNA-seq aligner. Bioinformatics 2013; 29:15–21.
101. Li Bo, Dewey Colin RSEM: accurate transcript quantification from RNA-Seq data with or without a reference genome. BMC Bioinformatics 2011;4(12):323. https://doi.org/10.1186/1471-2105-12-323.

Received April 6, 2021. Accepted August 3, 2021.

Correspondence
Address correspondence to: Phillip Karpowicz, PhD, Department of Biomedical Sciences, University of Windsor, 410 Sunset Avenue, Essex 275-2, Windsor, Ontario, Canada N9B 3P4. e-mail: Phillip.Karpowicz@uwindsor.ca.

Acknowledgments
The authors would like to thank members of the Karpowicz Laboratory for their support, Sharon Lavigne for logistic support, and David Weaver for helpful comments on the manuscript.

CRediT Authorship Contributions
Kyle Stokes, MSc (Formal analysis: Equal; Investigation: Lead; Writing – original draft: Supporting)
Malika Nunes, MSc (Investigation: Supporting)
Chantelle Trombley, MSc (Investigation: Supporting)
Danilo E. F. L. Flôres, PhD (Data curation: Lead; Formal analysis: Supporting)
Gang Wu, PhD (Data curation: Supporting; Formal analysis: Lead)
Zainab Taleb, MSc (Investigation: Supporting)
Abedalrhman Alkhateeb, PhD (Data curation: Supporting; Formal analysis: Supporting)
Suhrid Banskota, PhD (Investigation: Supporting)
Chris Harris, MSc (Investigation: Supporting)
Oliver P. Love, PhD (Investigation: Supporting; Supervision: Supporting)
Waliul I. Khan, PhD (Investigation: Supporting; Supervision: Supporting)
Luis Rueda, PhD (Formal analysis: Supporting; Supervision: Supporting)
John B. Hogenesch, PhD (Data curation: Supporting; Formal analysis: Supporting; Supervision: Supporting)
Phillip Karpowicz, PhD (Conceptualization: Lead; Investigation: Lead; Supervision: Lead)

Conflicts of interest
The authors disclose no conflicts.

Funding
Funded by the Natural Sciences and Engineering Research Council of Canada Alexander Graham Bell Scholarship (K.S.); Sao Paulo Research Foundation grant FAPESP 2019/04451-3 (D.F.); Mitacs Accelerate Postdoctoral Fellowship (A.A.); Canadian Institutes of Health Research grant PJT-156262 and the Natural Sciences and Engineering Research Council of Canada grant RGPIN-2019-06739 (W.I.K.); Natural Science and Engineering Research Council and the Canada Research Chairs program (O.P.L.); Natural Sciences and Engineering Research Council of Canada grant RGPIN-2019-04696 (L.R.); National Institute of Neurological Disorders and Stroke grant 5R01NS054794-13, National Heart, Lung, and Blood Institute grant 5R01HL138551-02, and the National Cancer Institute grant 1R01CA227485-01A1 (J.B.H.); and the Canadian Institutes of Health Research grant PJT-388014, Canada Foundation for Innovation/Ontario Research Fund, and the Ontario Institute for Regenerative Medicine, and Crohn's and Colitis Canada (P.K.). The contents of this article are solely the responsibility of the authors and may not represent the official views of the sponsoring agencies.